Ligand requirements for immunoreceptor triggering

Michael I. Barton, Rachel L. Paterson[1], Eleanor M. Denham[2], Jesse Goyette[3,4], P. Anton van der Merwe[4,5]

Sir William Dunn School of Pathology, University of Oxford, Oxford OX1 3RE

[1]Current address: Stemmatters, Biotecnologia e Medicina Regenerativa SA, Parque de Ciência e Tecnologia Avepark, Zona Industrial da Gandra, Barco, Portugal

[2]Current address: Enara Bio, The Magdalen Centre, Oxford Science Park, 1 Robert Robinson Avenue, Oxford OX4 4GA

[3]Current address: Department of Molecular Medicine, School of Biomedical Sciences, University of New South Wales, Sydney 2052, NSW, Australia

[4]These authors contributed equally

[5]Correspondence: anton.vandermerwe@path.ox.ac.uk

Abstract

Leukocytes interact with other cells using cell surface receptors. The largest group of such receptors are non-catalytic tyrosine phosphorylated receptors (NTRs), also called immunoreceptors. NTR signalling requires phosphorylation of cytoplasmic tyrosine residues by SRC-family tyrosine kinases. How ligand binding to NTRs induces this phosphorylation, also called NTR triggering, remains controversial, with roles suggested for size-based segregation, clustering, and mechanical force. Here we exploit a recently developed cell-surface generic ligand system to explore the ligand requirements for NTR triggering. We examine the effect of varying the ligand's length, mobility and valency on the activation of representative members of four NTR families: SIRPβ1, Siglec 14, NKp44 and TREM-1. Increasing the ligand length impairs activation via NTRs, despite enhancing cell-cell conjugation, while varying ligand mobility has little effect on either conjugation or activation. Increasing the valency of the ligand, while enhancing cell-cell conjugation, does not enhance activation at equivalent levels of conjugation. These findings are more consistent with a role for size-based segregation, rather than mechanical force or clustering, in NTR triggering, suggesting a role for the kinetic-segregation model.

Introduction

The cell surface of an immune cell or leukocyte presents many different receptors, which sense their environment through ligand binding (Barclay et al., 1997; Shilts et al., 2022; Springer, 1990). Many leukocyte receptors bind to ligands on the surface of other cells to mediate adhesion and/or transduce signals which regulate leukocyte function. These signals determine whether the leukocyte ignores or responds to the cell and influence the nature of the response. The largest class of such receptors are non-catalytic tyrosine-phosphorylated receptors (NTRs), which are also called immunoreceptors (Dushek et al., 2012). More than one hundred leukocyte receptors, in more than 20 families, can be classified as NTRs (Dushek et al., 2012). Because they regulate immune cell function, NTRs have roles in a wide range of diseases, and they are being exploited for therapeutic purposes. For example, synthetic NTRs (e.g. chimeric antigen receptors) and antibodies targeting NTRs or their ligands (e.g. checkpoint inhibitors) have become standard therapies for several forms of cancer (June and Sadelain, 2018; Sharma and Allison, 2015).

While NTRs have structurally diverse extracellular regions they all have, or are associated with signalling subunits that have, conserved tyrosine containing motifs in their cytoplasmic domains, such as the immunoreceptor tyrosine-based activation motif (ITAM) and immunoreceptor tyrosine-based switch motif (ITSM) (Dushek et al., 2012). These motifs are phosphorylated by SRC-family tyrosine kinases, which are tethered via acyl groups to the inner leaflet of the plasma membrane. This phosphorylation is

49 regulated by the receptor tyrosine phosphatases CD45 and CD148, which act on both SRC-kinases and
50 their substrates. While the extracellular regions of NTRs are structurally diverse, they are typically
51 smaller (4-10 nm) than many abundant cell surface molecules such as CD43, CD44, CD45, CD148 and
52 integrins, which range in size from 21-50 nm. When these size differences were first noted for the TCR
53 and its peptide-MHC (pMHC) ligand it was predicted that, when T cells contacted other cells, there
54 would be segregation of the TCR/pMHC complex from larger molecules like CD45 (Springer, 1990). This
55 observation, together with evidence that constitutive tyrosine phosphatase activity suppresses TCR
56 triggering in resting cells (O'Shea et al., 1992; Secrist et al., 1993), led to the proposal that TCR binding
57 to pMHC induced tyrosine phosphorylation of the TCR by trapping it in small regions of close contact
58 which exclude large receptor tyrosine phosphatases CD45 and CD148 but not the SRC-kinases (Davis and
59 Van der Merwe, 1996). This mechanism was subsequently termed the kinetic segregation (KS) model
60 (Van der Merwe et al., 2000). Subsequent studies from multiple laboratories using a wide range of
61 techniques have demonstrated that the KS mechanism plays a key role in TCR triggering (Burroughs et
62 al., 2006; Chang et al., 2016; Chen et al., 2021; Choudhuri et al., 2005; Cordoba et al., 2013; James and
63 Vale, 2012; Jenkins et al., 2023; Razvag et al., 2018; Schmid et al., 2016; Varma et al., 2006; Wilhelm et
64 al., 2021). Recently it has been shown that synthetic receptors based on the TCR, namely chimeric
65 antigen receptors (CARs), also appear to trigger by the KS mechanism, which has important implications
66 for the design of these receptors and selection of their target antigens (Xiao et al., 2022). Other
67 mechanisms that been proposed to contribute to TCR triggering are aggregation (Goyette et al., 2019) or
68 conformational change, with conformational change being either allosteric (Schamel et al., 2019) or
69 induced by mechanical force (Ma et al., 2008; Zhu et al., 2019).

70 The similarities in signalling between the TCR and other NTRs have led to the hypothesis that the KS
71 mechanism may contribute to triggering by other NTRs (Davis and Van der Merwe, 2006; Dushek et al.,
72 2012). Indeed, evidence for this has been reported for NKG2D in NK cells (Köhler et al., 2010), Dectin-1
73 (Goodridge et al., 2011)and FcγRs (Bakalar et al., 2018) in macrophages, and CD28 in T cells (Lim et al.,
74 2015). However, the diversity of NTRs and their ligands, and the fact that many NTR ligands have yet to
75 be identified, has hampered investigation of the triggering mechanism in a wider range of NTRs. We
76 have recently developed a generic ligand system based on the SpyTag/SpyCatcher split protein, which
77 enables cell-surface Streptactin to be used to engage any NTR incorporating a membrane-distal
78 StrepTagII peptide (Denham et al., 2019). Importantly, this generic ligand stimulated TCRs at the same
79 surface density as the native TCR ligand, validating it as a suitable model system for investigating NTR
80 triggering (Denham et al., 2019).

81 In the present study we used this generic ligand system to explore the ligand requirement for triggering
82 by representative members of 4 distinct NTR families (Figure 1A): Signal regulatory protein β1 (SIRPβ1),

83 Sialic acid-binding immunoglobulin-type lectin 14 (Siglec 14), Natural killer receptor 44 (NKp44) and
84 Triggering receptor expressed on myeloid cells 1 (TREM-1). SIRPβ1 is highly homologous to the
85 inhibitory receptor and therapeutic target SIRPα (Kharitonenkov *et al.*, 1997). SIRPβ1 and SIRPα are
86 examples of paired activatory/inhibitory NTRs (Dushek et al., 2012), with conserved extracellular regions
87 but distinct transmembrane and cytoplasmic domains. The native ligand of SIRPβ1 is unknown but it is
88 thought to promote phagocytosis in macrophages (Hayashi *et al.*, 2004). Siglec 14 is a member of the
89 sialic acid-binding Siglec family of receptors (Angata et al., 2006; Crocker et al., 2007). Siglec 14 and
90 Siglec 5 are paired activatory and inhibitory NTRs, respectively (Angata *et al.*, 2006). NKp44 is important
91 for the activation and cytotoxic activity of natural killer cells and reportedly binds a wide range of
92 ligands (Parodi et al., 2019). Finally, TREM-1 is an activatory member of a family of NTRs (Ford and
93 McVicar, 2009) that has been reported to bind peptidoglycan recognition protein 1 (PGLYRP1) (Read *et*
94 *al.*, 2015) and extracellular actin (Fu *et al.*, 2017). All four receptors associate with, and presumably
95 signal using, the ITAM-containing adaptor protein DAP12 (Lanier and Bakker, 2000).

96 To investigate the triggering mechanism used by these NTRs we examined the effect of changing ligand
97 size, mobility, and valency on activation. In addition to using the same generic ligand, we used the same
98 cell type and readouts for all NTRs, in order to facilitate comparisons between. Elongating the ligand
99 inhibited activation via these receptors despite enhancing receptor/ligand mediated cell-cell
100 conjugation. In contrast, changing the ligand mobility had little effect on conjugation or activation.
101 Finally, while increasing the ligand valency increased cell-cell conjugation as well as activation, it
102 decreased the level of activation at equivalent levels of cell-cell conjugation. Taken together, these
103 results are more consistent with a role for the KS mechanism in triggering by these NTRs, and do not
104 support a role for mechanical force or clustering.

105 Results

106 Varying ligand length

107 In the SpyTag-SpyCatcher system a covalent (isopeptide) bond spontaneously forms between Spytag
108 and SpyCatcher when they are mixed together (Zakeri *et al.*, 2012). In our previously described generic
109 ligand system (Denham et al., 2019), SpyTag is fused to the N-terminus of a transmembrane protein
110 expressed on ligand-presenting CHO cells, forming the ligand anchor, while SpyCatcher is fused to a
111 Strep-Tactin tetramer, which can have from one to four active binding sites, as required (Figure 1A). The
112 receptor is modified at its membrane-distal N-terminus to contain a Strep-tag II peptide, which binds
113 monovalent Strep-Tactin with a K_D of 43 μM (Denham et al., 2019). This is within the affinity range
114 typical of leukocyte cell-cell interactions (Van der Merwe and Barclay, 1994; Shilts et al., 2022).

115 To test the effect of ligand length on activation via NTRs, we produced CHO cells expressing either a
116 short or a long ligand anchor, where the latter includes a ~11 nm spacer comprising the four Ig domains
117 of CD4 (Figure 1A) (Wu et al., 1997). By titrating the monovalent Strep-Tactin SpyCatcher we produced a
118 panel of CHO cells with a range of binding sites. We used a previously described method to accurately
119 quantify the number of Strep-Tactin binding sites presented by these cells (Denham et al., 2019). This
120 involved measuring the maximum number of biotin binding sites and the K_D for Strep-Tactin SpyCatcher
121 coupling to cells (sFigure 1) and using these parameters to calculate the number of binding sites, as
122 described in the Materials and Methods.

123 We first measured the impact of ligand elongation on the receptor engagement using a cell-cell
124 conjugation assay as a readout. For receptor cells we used THP-1 cells expressing the SIRPβ1 receptor
125 with an N-terminal Strep-tag II peptide. THP-1 cells are a human monocytic cell line that is widely used
126 as a model for studying monocyte/macrophage function (Auwerx, 1991). They are a suitable model as
127 SIRPβ as well TREM-1, Siglec-14 and NKp44 are all known to be expressed on monocytes. The
128 conjugation assay involves mixing receptor and ligand cells stained with different fluorescent dyes and
129 measuring double positive events by flow cytometry (Figure 1B, upper right quadrants). As expected,
130 reducing the number of binding sites resulted in a decrease in the percentage of receptor cells in
131 conjugates (Figure 1B).

132 We then compared the conjugation efficacy of SIRPβ1 THP-1 cells mixed with short or long CHO cells
133 presenting different numbers of binding sites. When plotting conjugates against binding sites, cells
134 presenting the long ligand produced more conjugates (Figure 1C, left panel). This suggests that
135 increasing the ligand length promotes conjugate formation, which is consistent with other studies
136 suggesting that increasing the length of short (< 8 nm) cell surface ligands improves receptor
137 engagement (Choudhuri et al., 2005; Lim et al., 2015; Wild et al., 1999).

138 We next examined the effect of ligand length on SIRPβ1 mediated interleukin 8 (IL-8) production. IL-8 is
139 inflammatory chemokine produced monocytes in response to a wide variety of activation signals
140 (Baggiolini and Clark-Lewis, 1992), and it is widely-used a convenient and reliable readout of THP-1
141 activation, with low levels of basal release and a rapid increase following stimulation (Baqui et al., 1999).
142 Interestingly the long ligand stimulated less IL-8 production than the short ligand (Figure. 1C, middle
143 panel), despite mediating improved conjugate formation. To normalise for differences in conjugate
144 formation we plotted the functional IL-8 response against the percentage of receptor cells in conjugates
145 (Figure 1C, right panel). This confirmed that, at equivalent levels of conjugate formation, the long ligand
146 induced lower levels of IL-8 production.

147 We performed conjugation and stimulation assays on other NTRs (Siglec 14, NKp44 and TREM-1) using
148 the short or long generic ligand (Figure 2). As in the case of SIRPβ1, the results for NKp44 and TREM-1
149 show an increase in conjugation efficacy when binding to the long ligand compared to the short ligand
150 (Figure 2, left panels). This was not the case for Siglec 14, where no difference was seen (Figure 2B, left
151 panel). Elongation of the ligand impaired activation of IL-8 release via all four NTRs, both before and
152 after normalising for conjugate formation (Figure 2, centre and right panels, respectively).

153 One likely explanation for the effect of ligand length on activation efficiency is that increasing the ligand
154 length increases the length of the NTR/ligand complex. If this is the case, activation should also be
155 reduced by increasing the length of the NTRs. The extracellular regions of SIRPβ1 and Siglec 14 each
156 contain 3 immunoglobulin superfamily (IgSF) domains, whereas the extracellular regions of NKp44 and
157 TREM-1 only have 1 IgSF domain (Figure 1A). To examine whether this size difference had a measurable
158 impact we reanalysed the data in Figure 2 to enable comparison of conjugation and activation via NTRs
159 exposed to the same ligand (sFigure 3). Short NTRs (NKp44 and TREM-1) mediated lower levels of
160 conjugation (sFigure 3, left panels) but high levels of stimulation when normalised for conjugation
161 (sFigure 3, right panels), and this was observed with both short (sFigure 3A) and long (sFigure 3B)
162 ligands. Taken together, these data show that elongation of these NTR/ligand complexes attentuates
163 activation via these four NTRs.

164 **Varying ligand mobility**

165 We next examined the effect of varying the ligand anchor on NTR activation. We compared ligand
166 anchors based on the transmembrane and cytoplasmic domains of CD80, and CD43 and the
167 glycosylphosphatidylinositol (GPI) anchor of CD52. The CD43 cytoplasmic domain interacts with the
168 actin cytoskeleton though Ezrin/Radixin/Moesin (ERM) proteins (Yonemura *et al.*, 1998), and so is likely
169 to be more firmly anchored. In contrast, CD52 is a GPI anchored protein and thus less firmly anchored,
170 and presumably more mobile (Figure 3A). To examine mobility, SpyCatcher-GFP was coupled to ligand
171 anchors and fluorescence recovery after photobleaching (FRAP) performed. As expected, the CD52
172 anchor conferred greater mobility than the CD80 or CD43 anchor, which were similar (sFigure 4A, Figure
173 3B).

174 We next compared the effect of changing the ligand mobility on conjugation with and stimulation of
175 SIRPβ1 expressing THP-1 cells. It was not possible to attain as high a level of binding sites on the CD43
176 and CD52 ligand anchor cells but comparison was possible over a reasonable range. CD52 and CD43
177 anchored ligands induced similar levels of conjugate formation (Figure 3C, top panel) and IL-8 release
178 (Figure 3C, middle panel) at comparable levels of binding sites. CD52 anchored ligand induced slightly
179 less IL-8 release than CD43 anchored ligands when plotted against levels of conjugation (Figure 3C,

180 bottom panel). However this difference was small and could be the result of faster turnover of the CD52
181 anchored ligand (sFigure 5), which would reduce engagement during the 20 h stimulation. While the
182 CD80 anchored ligand was less potent at mediating conjugation and IL-8 release, this was not a
183 consequence of differences in lateral mobility which was similar to the lateral mobility of the CD43
184 anchored ligand (Figure 3B). Taken together, these results suggest that changes in the ligand mobility do
185 not affect SIRPβ1 mediated conjugation or triggering.

186 **Varying ligand valency**

187 Since ligand-induced clustering of receptors is often assumed to be the mechanism of receptor-
188 activation, we next examined the effect of increasing the valency of the ligand from 1 to 4 by using a
189 tetravalent form of Strep-Tactin Spycatcher. As expected, conjugation with tetravalent instead of
190 monovalent Strep-Tactin Spycatcher resulted in a four-fold increase in the number of binding sites
191 (sFigure 6). We then compared the ability of monovalent and tetravalent ligand to mediate conjugation
192 and induce IL-8 secretion from THP-1 cells expressing the 4 different NTRs. Tetravalent ligand induced
193 conjugation via all 4 NTRs at lower ligand binding site numbers than monovalent ligand (Figure 4, left
194 panels), indicating that increasing the ligand valency increases NTR binding, presumably by increasing
195 avidity. Increasing the valency enabled activation of all four receptors, as measured by IL-8 release, at
196 much lower ligand binding sites (Figure 4, middle panels). However, after controlling for increased
197 conjugate formation, tetravalent ligand was actually less effective than monovalent ligand at stimulating
198 IL-8 release at equivalent levels of conjugation (Figure 4, right panels). The same result was observed
199 with the CD80, CD43 and CD52 ligand anchors (sFigure 7 and 8). These results indicate that, while
200 increasing the valency of a cell surface-associated ligand enhances binding to NTRs, it does not increase
201 activation via NTRs.

202 We next investigated whether activation of NTR by the high avidity tetravalent Strep-Tactin SpyCatcher
203 was sensitive to ligand length. THP-1 cells expressing four representative NTRs were exposed to CHO
204 cells presenting tetravalent Strep-Tactin SpyCatcher on either short or long CD80 anchors (Figure 5). The
205 short ligands were less effective at mediating conjugation than the long ligand for two (SIRPβ1 & NKp44)
206 of the four NTRs (Figure 5, left panels), but more effective at stimulating IL-8 production for three of the
207 four NTRs (SIRPβ1, NKp44 and TREM-1), both before (Figure 5, centre panels) and after (Figure 5, right
208 panels) controlling for conjugate formation. These results show that even high avidity NTR/ligand
209 interactions remain sensitive to ligand length for three of the four NTRs studied here.

210 ## Discussion

211 We have exploited our previously described generic cell surface ligand system (Denham et al., 2019) to
212 explore the effects of varying ligand length, mobility, and valency on activation of four NTRs, SIRPβ1,
213 Siglec-14, NKp44 and TREM-1. One advantage of this system is that it enables titration of ligand surface
214 density, enabling detection of quantitative differences in the ability of cell-surface ligands to mediate
215 conjugation and stimulation. A second advantage is that it enables multiple NTRs to be assessed using
216 the same set of ligands, increasing throughput and facilitating comparisons between NTRs. Comparison
217 was also enabled by expressing them in the same cell type and using the same functional readout. A
218 third advantage is that it enables analysis of orphan NTRs, such as SIRPβ1, whose ligands have yet to be
219 identified.

220 Our first key finding is that elongation of generic ligands abrogated activation of all four NTRs. This was
221 not a consequence of decreased binding as elongated ligands mediate enhanced cell-cell conjugation.
222 While this contrasted with results in a supported lipid bilayer (SLB) system, in which elongation of CD48
223 abrogated CD2 binding (Milstein et al., 2008), it is consistent with results obtained with cell surface
224 expressed ligands, including CD48 (Choudhuri et al., 2005; Köhler et al., 2010; Lim et al., 2015; Wild et
225 al., 1999). A likely explanation for this is that ligands on cell surfaces, unlike ligands on SLBs, are crowded
226 by the larger molecules present at high densities. Our finding that long NTRs were less effectively
227 activated than short NTRs suggest that the increased NTR/ligand length abrogates NTR signalling. These
228 data are most consistent with the KS mechanism of NTR triggering (Davis and Van der Merwe, 2006),
229 since increasing the NTR/ligand length would be expected to increase the intermembrane distance and
230 thus reduce segregation of inhibitory receptor tyrosine phosphatases such as CD45 from the engaged
231 NTR (Choudhuri et al., 2005). Numerous studies have confirmed that increasing receptor/ligand length
232 abrogates CD45 segregation from engaged NTRs (Al-Aghbar et al., 2018; Bakalar et al., 2018; Chen et al.,
233 2017; Choudhuri et al., 2005; Lim et al., 2015; Xiao et al., 2022). In one of these studies an elongated
234 high affinity TCR ligand, derived from the OKT3 monoclonal antibody, was able to activate TCRs despite
235 less efficient exclusion of CD45 (Al-Aghbar et al., 2018). However, no titration of the ligand number was
236 performed, and a lower affinity variant of the same ligand was unable to activate T cells (Al-Aghbar et
237 al., 2018).

238 An alternative explanation for our finding that elongation abrogates activation through NTRs is that this
239 could decrease the level of force experienced by the NTR upon ligand engagement (Li et al., 2010).
240 These data are therefore also consistent with models of NTR triggering postulating that a mechanical
241 force imposed upon ligand binding alters the conformation of the NTR (Ma et al., 2008; Zhu et al., 2019).
242 However, whether changing ligand length affects the force experienced by an NTR has yet to be

243 confirmed, and it remains unclear how such a conformational change of NTRs could be transmitted
244 through the membrane to enhance phosphorylation of their cytoplasmic domains. Such a mechanism is
245 difficult to reconcile with enormous structural variability of NTRs (Dushek et al., 2012) and the fact that
246 chimeric NTRs such as CARs tolerate extensive variation in the regions (hinge, transmembrane and
247 cytoplasmic domains) that couple their ligand binding domains with their tyrosine-containing signalling
248 motifs (Labanieh and Mackall, 2023; Sadelain, 2016).

249 A second key finding is that changing the mobility of the ligand anchor had little impact on its ability
250 mediate activation via NTRs. The CD52 anchor comprises a lipid (GPI) which we show confers greater
251 lateral mobility. While there is only a ~2 fold change in mobility, it should be noted that membrane
252 diffusion in cells is far slower than in model membranes, likely because it is impaired by membrane
253 proteins that associate with the cortical actin cytoskeleton, which have been termed 'picket fences'
254 (Jacobson et al., 2019; Kusumi et al., 2011). A lipid anchor also allows a ligand to be more easily
255 extracted from the plasma membrane by force. Thus, the amount of force that can be exerted on an
256 NTR, both tangential and perpendicular to the membrane, should be lower with lipid-anchored than a
257 transmembrane-anchored ligand, such as CD43, able to bind to the actin cytoskeleton through ERM
258 proteins. Thus, our finding that CD43 and CD52 anchors were similarly effective at activating an NTR
259 does not support a role for mechanical force in triggering for these NTRs. We note, however, that we did
260 not directly measured force. Much stronger evidence against a role for force was reported by Göhring et
261 al. (2021), who showed that changing the lateral mobility of the TCR ligand in an SLB system by ~1000
262 fold had no effect on TCR triggering despite substantially changing the force experienced by the TCR
263 (Göhring et al., 2021).

264 The third key finding is that increasing the valency of the NTR ligand did not increase activation of the
265 NTR after controlling for enhanced NTR binding, as assessed by cell-cell conjugation. This result
266 contrasts with the findings obtained with soluble NTR ligands such as cross-linked antibodies and natural
267 ligands engineered to be multivalent, where increasing the valency is required for NTR triggering
268 (Boniface et al., 1998; Cochran et al., 2000). One possible explanation for this discrepancy between the
269 effect of valency with soluble and surface associated ligand is that a soluble multivalent ligand could, by
270 forming clusters of NTRs, exclude molecules with bulky ectodomain, such as CD45, from clustered NTRs,
271 whereas soluble monovalent ligands are unable to do this. In contrast, even a monovalent surface-
272 associated ligand can trap the NTR in zones of a close intermembrane contact from which CD45 and
273 CD148 are excluded. While our finding that tetravalent ligands are less effective at activating NTRs than
274 monovalent ligands at equivalent levels of NTR binding requires confirmation and further analysis, the
275 fact that increased valency does not enhance NTR triggering argues against aggregation as the primary
276 mechanism of physiological NTR triggering. Further evidence against this model is that almost all cell

277 surface NTRs ligands that have been identified to date are monovalent (Dushek et al., 2012). In contrast,
278 cell surface receptors known to signal by binding induced multimerisation, such as class III tyrosine
279 kinase receptors (Ullrich and Schlessinger, 1990) and TNF receptor superfamily members (Locksley et al.,
280 2001), typically have multivalent ligands.

281 Our finding that elongation of a tetravalent generic ligand did not impair activation via Siglec 14, while it
282 did impair activation via the three other NTRs, suggests that, for some NTRs, increasing ligand valency
283 can bypass the need for the KS mechanism. It is noteworthy that some Siglec family members, including
284 the Siglec-14 paired receptor Siglec-5 (Cornish et al., 1998), are able to form disulphide linked dimers.
285 Dimeric Siglec-14 would allow formation of large 'zipper-like' aggregates with tetravalent generic ligand,
286 enabling exclusion of CD45 and CD148 without needing the KS mechanism.

287 Taken together, our finding that activation via NTRs is abrogated by ligand elongation and aggregation
288 and unaffected by the mobility of the ligand anchor supports our hypothesis that NTRs signal by the KS
289 mechanism. While our results focus only on four representative NTRs, these results are likely to apply to
290 a larger number of NTRs, including other members of the Siglec and TREM families and NTRs from other
291 families that signal via the DAP-12 adaptor (Lanier, 2008). As reviewed in the Introduction, there is
292 already evidence that many NTRs that do not associate with DAP12, including the TCR, NKG2D, CD28,
293 and FcγR, exploit the KS mechanism for triggering. Taken together with the results presented in this
294 paper, this suggests that the KS mechanism is used by NTRs which signal through intrinsic tyrosine
295 motifs (CD28, FcγRI and FcγRII) and a variety of signalling subunits (DAP12, DAP10, CD3δεγ, CD247, and
296 FcRγ).

297 One limitation of the present work is that we used artificial ligands rather than native ligands. While we
298 have previously validated the generic ligand system for the T cell receptor (Denham et al., 2019), this is
299 more challenging for other NTRs, as their ligands cannot easily be titrated. Our recent development of
300 Combicells (Patel et al., 2023), which exploit the SpyCatcher/SpyTag system to present native ligand on
301 antigen presenting cells, should enable our key results to be confirmed with native ligands, where
302 known. A second limitation, which is a consequence of the system used, is lack of imaging data of the
303 interface between THP-1 cells and CHO cells. Advanced microscopy, beyond the scope of this study, is
304 likely needed to image the molecular events in the microvilli-like structures and close contact areas
305 involved in NTR triggering at cell-cell interfaces (Jenkins et al., 2023; Jung et al., 2021; Stinchcombe et
306 al., 2023). A third limitation is that we only test one prediction of the KS model, that elongation of the
307 receptor/ligand complex will abrogate NTR triggering. Other predictions of the KS model should be
308 tested in future work.

309 ## Material and Methods

310 **Constructs**

311 Receptors

312 Receptor sequences for SIRPβ1, Siglec 14, NKp44 and TREM-1 were inserted into the pHR-SIN-BX-Strep-
313 tag II plasmid as described by (Denham *et al.*, 2019). The same constructs containing the DAP12 adaptor
314 protein was also used.

315 Ligand anchors

316 For the ligand anchors DNA encoding the Igk leader sequence (bold), HA tag (italics), SpyTag
317 (underlined) bracketed by GGS linkers, and the hinge, transmembrane and intracellular regions of
318 mouse CD80, mouse CD43, or human CD52 (italics underlined) was inserted into the vector pEE14. To
319 express the long ligand anchor DNA encoding human CD4 (italics bold) was inserted between the SpyTag
320 and CD80 hinge. This included an R to D point mutation (underlined) to prevent CD4 binding MHC class
321 II. After expression CD52 anchor is cleaved and linked to GPI anchor at the serine residue marked in bold

322 CD80 anchor (short):

323 **M E T D T L L L W V L L L W V P G S T G D** *Y P Y D V P D Y A* T G G S A H I V M V D A Y K P T K G G S G G S *H*
324 *V S E D F T W E K P P E D P P D S K N T L V L F G A G F G A V I T V V V I V V I I K C F C K H R S C F R R N E A S*
325 *R E T N N S L T F G P E E A L A E Q T V F L*

326 CD80 anchor (long):

327 **M E T D T L L L W V L L L W V P G S T G D** *Y P Y D V P D Y A* T G G S A H I V M V D A Y K P T K G G S G G S ***K***
328 ***V V L G K K G D T V E L T C T A S Q K K S I Q F H W K N S N Q I K I L G N Q G S F L T K G P S K L N D*** **D** ***A D S***
329 ***R R S L W D Q G N F P L I I K N L K I E D S D T Y I C E V E D Q K E E V Q L L V F G L T A N S D T H L L Q G Q S***
330 ***L T L T L E S P P G S S P S V Q C R S P R G K N I Q G G K T L S V S Q L E L Q D S G T W T C T V L Q N Q K K V***
331 ***E F K I D I V V L A F Q K A S S I V Y K K E G E Q V E F S F P L A F T V E K L T G S G E L W W Q A E R A S S S K***
332 ***S W I T F D L K N K E V S V K R V T Q D P K L Q M G K K L P L H L T L P Q A L P Q Y A G S G N L T L A L E A K***
333 ***T G K L H Q E V N L V V M R A T Q L Q K N L T C E V W G P T S P K L M L S L K L E N K E A K V S K R E K A V***
334 ***W V L N P E A G M W Q C L L S D S G Q V L L E S N I K V L P T R S*** *H V S E D F T W E K P P E D P P D S K N T*
335 *L V L F G A G F G A V I T V V V I V V I I K C F C K H R S C F R R N E A S R E T N N S L T F G P E E A L A E Q T V*
336 *F L*

337 CD43 anchor:

338 **M E T D T L L L W V L L L W V P G S T G D** *Y P Y D V P D Y A T G G S* A H I V M V D A Y K P T K G G S G G S *Q*
339 *E S S G M L L V P M L I A L V V V L A L V A L L L L W R Q R Q K R R T G A L T L S G G G K R N G V V D A W A*
340 *G P A R V P D E E A T T T S G A G G N K G S E V L E T E G S G Q R P T L T T F F S R R K S R Q G S L V L E E L K*
341 *P G S G P N L K G E E E P L V G S E D E A V E T P T S D G P Q A K D E A A P Q S L*

342 CD52 anchor:

343 **M E T D T L L L W V L L L W V P G S T G D** *Y P Y D V P D Y A T* G G S A H I V M V D A Y K P T K G G S G G S *D*
344 *T S Q T S S P* ***S*** *A S S N I S G G I F L F F V A N A I I H L F C F S*
345

346 Soluble proteins

347 Strep-Tactin-SpyCatcher sequence:

348 Strep-Tactin is underlined, SpyCatcher is in italics and the polyaspartate sequence is in bold.

349 M A E A G I T G T W Y N Q L G S T F I V T A G A D G A L T G T Y V T A R G N A E S R Y V L T G R Y D S A P A T
350 D G S G T A L G W T V A W K N N Y R N A H S A T T W S G Q Y V G G A E A R I N T Q W L L T S G T T E A N A
351 W K S T L V G H D T F T K V K P S A A S **D D D G D D D G D D D D** *S A T H I K F S K R D E D G K E L A G A*
352 *T M E L R D S S G K T I S T W I S D G Q V K D F Y L Y P G K Y T F V E T A A P D G Y E V A T A I T F T V N E Q G*
353 *Q V T V N G K A T K G D A H I*

354 Strep-Tactin sequence:

355 M A E A G I T G T W Y N Q L G S T F I V T A G A D G A L T G T Y V T A R G N A E S R Y V L T G R Y D S A P A T
356 D G S G T A L G W T V A W K N N Y R N A H S A T T W S G Q Y V G G A E A R I N T Q W L L T S G T T E A N A
357 W K S T L V G H D T F T K V K P S A A S

358 Dead Streptavidin sequence:

359 Bold amino acids mark substitutions in order to prevent binding to Strep tag II or biotin.

360 M A E A G I T G T W Y **A** Q L G **D** T F I V T A G A D G A L T G T Y E **A** A V G A E S R Y V L T G R Y D S A P A T D
361 G S G T A L G W T V A W K N N Y R N A H S A T T W S G Q Y V G G A E A R I N T Q W L L T S G T T E A N A W
362 K S T L V G H D T F T K V K P S A A S

363 GFP-SpyCatcher

364 The GFP-SpyCatcher construct was described in (Denham *et al.*, 2019).

365 **THP-1 cell lines**

366 THP-1 cells (ATCC #TIB 202) were maintained in RPMI-1640 media (Sigma-Aldrich #R8758)
367 supplemented with 10% foetal bovine serum (FBS) and 1 in 100 penicillin/streptomycin (Thermo Fisher
368 Scientific #15140122) at 37 °C in a 5% CO2 containing incubator.

369 **CHO cell lines**

370 Chinese Hamster Ovary (CHO) mock cells were maintained in DMEM (Sigma-Aldrich #D6429)
371 supplemented with 5% FBS and 1 in 100 penicillin/streptomycin. CHO ligand anchor cells (short and
372 long) were maintained in L-Glutamine-free DMEM (Sigma-Aldrich #D6546) supplemented with 10%
373 dialysed FBS (dialysed three times against 10 L PBS), 1 in 100 penicillin/streptomycin, 1x GSEM
374 supplement (Sigma-Aldrich #G9785) and 50 µM L-Methionine sulfoximine (Sigma-Aldrich #M5379).

375 **Lentiviral transduction of THP-1 cells**

376 Either receptor-expressing lentivector alone, or with the DAP12 adaptor-expressing lentivector, was co-
377 transfected with the lentiviral packaging plasmids pRSV-Rev (Addgene plasmd #12253), pMDLg/pRRE
378 (Addgene plasmd #12251) and pMD2.g (Addgene plasmd #12259) into HEK293T cells using X-
379 tremeGENETM HP (Sigma-Aldrich 6366546001) as per the manufacturer's instructions. Two days after
380 transfection, viral supernatants were harvested, filtered (0.45 µM syringe filter) and used for the
381 transduction of THP-1 cells in the presence of 5 µg mL^{-1} Polybrene.

382 **Analysing receptor and adaptor expression using flow cytometry and cell sorting by Fluorescence-**
383 **Activated Cell Sorting (FACS)**

384 Cells were analysed for receptor surface expression by flow cytometry using anti-Strep-tag II antibody
385 StrepMAB™ directly conjugated to Oyster 645 (IBA Lifesciences #2-1555-050), or unconjugated
386 StrepMAB™ (IBA Lifesciences #2-1507-001) with anti-mouse IgG1 antibody Alexa Fluor 647 (Thermo
387 Fisher Scientific #A-21240), on a Cytek DxP8. Introduced adaptor expression was tested via expression of
388 EmGFP encoded on the adaptor lentivector. Cells were sorted for matched high expression of receptor
389 plus introduced adaptor by fluorescence-activated cell sorting (FACS) (MoFlo Astrios, Beckman Coulter).

390 **Transfection of CHO cells with various ligand anchors**

391 CHO cells were transfected with either pEE14 (CHO mock) or pEE14-ligand anchor (CHO ligand anchor)
392 using Xtreme-GENE 9™ as per the manufacturer's instructions. Transfected lines were cultured in the
393 appropriate selection media after 48 hours.

394 **Checking ligand anchor expression by flow cytometry**

395 CHO Cells were analysed for ligand anchor surface expression by flow cytometry using anti-HA-Tag
396 antibody Alexa Fluor 647 (6E2; Cell Signalling Technology). Alternatively, cells were coupled with
397 saturating concentration of monovalent StrepTactin SpyCatcher. Biotin ATTO 647 was then added at 2
398 µM for 30 minutes. The cells were washed 3 times in PBS 1%BSA before they were fixed in PBS 1%
399 formaldehyde and analysed via flow cytometry.

400 **Expression and purification of monovalent and tetravalent Strep-Tactin-SpyCatcher**

401 Strep-Tactin SpyCatcher and dead streptavidin (monovalent) or Strep-Tactin SpyCatcher and Strep-
402 Tactin (tetravalent) expressed in Escherichia coli BL21-CodonPlus (DE3)-RIPL cells (Agilent Technologies
403 #230280) were combined and refolded from inclusion bodies. Inclusion bodies were washed in
404 BugBuster (Merck Millipore #70921) supplemented with lysozyme, protease inhibitors, DNase I and
405 magnesium sulphate as per the manufacturers' instructions. Subunits were then mixed at a 3:1 molar
406 ratio to improve the yield of the desired tetramer. The subunits were refolded by rapid dilution in cold
407 PBS and contaminates removed via precipitation using ammonium sulphate before additional
408 ammonium sulphate was added to precipitate the desired tetramer. Precipitated protein was
409 resuspended in 20 mM Tris pH 8.0, filtered (0.22 µm syringe filter), and loaded onto a Mono Q HR 5/5
410 column (GE Healthcare Life Sciences). Desired tetramers were eluted using a linear gradient of 0-0.5 M
411 NaCl in 20 mM Tris pH 8.0, concentrated, and buffer exchanged into 20 mM MES, 140 mM NaCl pH 6.0
412 (Denham *et al.*, 2019).

413 **Coupling CHO generic ligand cells**

414 Ligand anchor expressing or mock transduced CHO cells were incubated with various concentrations of
415 monovalent or tetravalent Strep-Tactin SpyCatcher in 20 mM MES, 140 mM NaCl, pH 6.0 and 1% BSA for
416 10 minutes at RT. Unbound Strep-Tactin SpyCatcher was removed by washing three times with PBS 1%
417 BSA.

418 **FACS Sorting of ligand anchor expressing CHO cells**

419 CHO short and long cells were coupled with a saturating concentration of monovalent Strep-Tactin
420 SpyCatcher. Biotin ATTO 647 (ATTO-TEC #AD 647-71) was then added at 2 µM for one hour and the
421 excess washed off with PBS 1 % BSA. The short and long CHO cells were then sorted for matched
422 expression of atto 647 signal corresponding to the expression level of ligand anchor using FACS (MoFlo
423 Astrios, Beckman Coulter).

424 **Biotin-4-fluorescein quenching assay**

425 The valency of purified monovalent and tetravalent Strep-Tactin SpyCatcher was measured using biotin-
426 4-fluorescein (Sigma-Aldrich #B9431-5MG) which when bound to Strep-Tactin become quenched.
427 Monovalent and tetravalent Strep-Tactin SpyCatcher was incubated with a titration of biotin-4-
428 fluorescein in black, opaque plates for 30 minutes at RT in PBS 1% BSA. Fluorescence was measured (λ_{ex}
429 485 nm, λ_{ex} 520 nm) using a plate reader. Fluorescence values were corrected for background
430 fluorescence before analysis. Negative control (buffer alone) data were fitted with the linear regression.
431 Sample data was fitted with a segmental linear regression, equation below, where X is the biotin-4-
432 fluorescein concentration, Y is fluorescence (AU), X0 is the biotin-4-fluorescein concentration at which
433 the line segments intersect. Slope1 was constrained to zero and is the gradient of the first line segment,
434 slope2 is the gradient of the second line segment. Intercept1 was constrained to zero and is the Y value
435 at which the first line segment intersects the Y axis. Slope2 was constrained to the gradient given by the
436 linear regression of the negative control.

437 $$Y1 = Intercept\ 1 + Slope1 * X$$

438 $$Y\ at\ X0 = Slope1 * X0 + Intercept1$$

439 $$Y2 = Y\ at\ X0 + Slope2 * (X - X0)$$

440 $$Y = IF\ (X < X0, Y1, Y2)$$

441 The X0 value was converted into an estimate of the number of biotin-binding sites per tetramer using
442 the concentration of Strep-Tactin SpyCatcher added and assuming complete binding of biotin-4-
443 fluorescein.

444 **Measurement of ligand binding sites on cells**

445 Ligand-anchor expressing or mock transduced CHO cells (3 x 10^6) were pre-incubated with a saturating
446 concentration of monovalent or tetravalent Strep-Tactin SpyCatcher. The above biotin-4-fluorescein
447 quenching assay was performed in the same manner but with a known number of cells. The X0 term
448 (calculated from the curve fit using equations above) was converted to the average number of binding
449 sites per cell using the equation below, where N is the average number of ligands per cell, X0 is the
450 saturation concentration of biotin-4-fluorescein extracted (M), V is the sample volume (L), N_A is
451 Avogadro's constant and C is the number of cells in the sample.

452 $$N = \frac{X0 * V * N_A}{C}$$

453 To measure relative levels of coupled SpyCatcher per cell, ligand cells were pre-incubated with a range
454 of concentrations of monovalent or tetravalent Strep-Tactin SpyCatcher or buffer alone (as a negative
455 control) before being incubated with 2 µM biotin ATTO 488 (ATTO-TEC #AD 488-71) pre-mixed with 40
456 µM biotin for 30 minutes at RT. The presence of biotin minimises the self-quenching activity of ATTO dye
457 observed with tetravalent Strep-Tactin. Cells were analysed by flow cytometry and the gMFI when cells
458 were incubated with buffer alone instead of Strep-Tactin SpyCatcher was subtracted from all
459 corresponding sample gMFI values. These values were then fitted with the single site binding model,
460 equation below, where Y is the gMFI (AU), Bmax is the maximum specific SpyCatcher binding indicated
461 by gMFI in AU, X is the [Streptactin-SpyCatcher] added (M) and K_D is the [SpyCatcher] that yields 50%
462 maximal binding to CHO cells (M).

463 $$Y = \frac{Bmax * X}{Kd + X}$$

464 To convert Y values into the average number of binding sites per ligand cell, the number of binding sites
465 per cell at saturating monovalent/tetravalent Strep-Tactin SpyCatcher concentration calculated in the
466 biotin-4-fluorescein assay was substituted into the equation above as Bmax. Y values were then re-
467 calculated following this adjustment. This method was followed in each independent experiment and
468 then an average value for the K_D and Bmax was used when combining replicates.

469 **Fluorescent recovery after photobleaching**

470 CHO cells (1 x10^5) expressing the three ligand anchors (CD80, CD43 and CD52) were transferred to a 35
471 mm glass bottom dish one day before imaging. To prepare cells for imaging each dish was washed 3
472 times with coupling buffer plus 10 % FBS. SpyCatcher-GFP was then added in excess (approximately 10
473 µM) and left for 10 minutes. Before washing the cells three times in PBS 1 % BSA 10 % FBS. Cells were
474 transferred to the Olympus FV1200 laser scanning microscope with 37 °C chamber for equilibration. The
475 60X magnification lens was used to locate cells spread over the glass coverslip. A small area of the cell
476 (approximately 10 %) was selected a few control images were taken before a 20 second bleach
477 performed. A time lapse series of images was then taken to track the recovery of the GFP signal.

478 Time lapse image series were imported into ImageJ for analysis. For each time lapse the bleach area was
479 selected (bleach) along with a control area which was taken to be the rest of the cell contact with the
480 glass (control area) and a negative control area around the outside of the cell (negative). Firstly, the
481 intensity from the negative area was subtracted from the bleach and control area. The bleach area was
482 then divided by the control area for each time frame and these values were normalised to the control
483 image before the bleach was performed. These values were then plotted against time and the equation
484 below used to find the half time for each ligand anchor.

485 $$Y = Y0 + (Plateau - Y0) * (1 - e^{-K*x})$$

486 Where Y0 is the value when X (time) is zero, Plateau is the Y value at infinite times and K is the rate
487 constant from which the half time is derived.

488 The half time value could then be converted into the diffusion coefficient using the equation below
489 (Soumpasis, 1983).

490 $$Diffusion\ coefficient = 0.224 * r^2 / half\ time$$

491 Where 0.224 is a constant for a circular bleach area, r is the radius of the bleach area, and the half time
492 is the derived from fitting the one phase association equation to the bleach recovery above.

493 **Ligand turnover**

494 CHO ligand anchor cells were incubated with 15 µM monovalent Strep-Tactin SpyCatcher (or buffer
495 alone) as described above and incubated at 37 °C to match stimulation assays for the time points
496 indicated. Cells were analysed for generic ligand surface expression using ATTO 488 biotin as above and
497 normalised to the geometric fluorescence intensity value at time 0. To calculate the decay, the gMFI
498 values were fitted with the equation below where Y0 is the Y value when X = 0, Plateau is the Y value at
499 which the curve reaches a plateau, X is time in minutes, and K is the rate constant in inverse minutes.

500 $$Y = (\mathrm{Y0} - \mathrm{Plateau}).e^{-K.X} + \mathrm{Plateau}$$

501 **IL-8 production**

502 CHO ligand anchor cells (2 x 10^5) coupled with either monovalent/tetravalent Strep-Tactin SpyCatcher or
503 buffer alone were mixed with single Strep-tag II tagged receptor and adaptor expressing THP-1 or
504 untransduced THP-1 cells (1 x 10^5) in DMEM 5% FBS, 1 in 100 penicillin/streptomycin, 2 µg mL^{-1} avidin.
505 Cells were incubated in a 37 °C 10% CO2 containing incubator for 20 hours. Supernatants were
506 harvested and assayed for IL-8 by ELISA following manufacturer's instructions (Thermo Fisher Scientific
507 #88808688).

508 **Conjugation assays**

509 Ligand cells were stained with CellTrace Far Red (Thermo Fisher Scientific #C34564) at a final
510 concentration of 1 µM in PBS at a density of 1 x 10^6 cells per ml. THP-1 receptor cells were stained with
511 CellTrace Violet (Thermo Fisher Scientific #C34557) at a final concentration of 1 µM in PBS for 20
512 minutes. CHO Ligand cells (4 x 10^5) coupled with either monovalent/tetravalent Strep-Tactin SpyCatcher
513 were mixed with (2 x 10^5) THP-1 cells in PBS 1 % BSA on Ice for 1 hour. Conjugation efficacy was
514 analysed by flow cytometry.

515 Due to experimental constraints stimulation and conjugation assays were completed on successive days.
516 However, we confirmed that the same result was observed when the stimulation and conjugation assays
517 were performed in parallel on the same day by splitting the cells in half for each assay (Supplementary
518 Figure 2)

519 **Data analysis**

520 For receptor stimulation assays, IL-8 concentrations in negative controls (where CHO cells were pre-
521 incubated with buffer alone instead of Strep-Tactin SpyCatcher) were subtracted from corresponding
522 sample IL-8 concentrations to correct for background levels. Dose-response curves were then fitted with
523 the below equation where Y is the measured cell response (pg mL^{-1}), Bottom and Top are the minimum
524 and maximum cell response respectively (pg mL^{-1}), EC50 is the number of binding sites per cell that
525 yields a half maximal response, X is the number of binding sites per cell and Hill slope relates to the
526 steepness of the curve.

527 $$Y = Bottom + \frac{(X^{Hillslope})(Top - Bottom)}{(X^{Hillslope} + EC50^{Hillslope})}$$

528 For conjugate assays the percentage of THP-1 cells forming conjugates was calculated using the formula
529 below. The data was then fit using the same dose response equation above except with X being the
530 percentage of THP-1 cells in conjugates, normalized where indicated.

531 $$Receptor\ cells\ in\ Conjugates\ (\%) = \frac{Double\ positive\ events}{Receptor\ only\ events + Double\ positive\ events} * 100$$

532 To plot stimulation as a function of conjugation the average number of binding sites used in the
533 stimulation assay were interpolated from the fit of the conjugation data using the four parameter dose
534 response model. The IL-8 values from the stimulation were then plotted against the interpolated values
535 of conjugate formation.

536 To enable the results from multiple experiments to be included in single plots data were normalised.
537 This increased the statistical power of the experiments by increasing the number of data points for each
538 fit. For statistical analysis F tests, t tests ANOVA were performed as appropriate and results presented
539 with the following symbols: ns, not significant ; * , $p < 0.05$; **, $p < 0.01$; ***, $p < 0.001$; ****, $p <$
540 0.0001.

541 ## Data availability statement

542 All data supporting the findings of this study are available within the paper. Should any raw data
543 files be needed they are available from the corresponding authors upon reasonable request.

Acknowledgements

We acknowledge Mark Howarth for providing Strep-Tactin, streptavidin, SpyTag and SpyCatcher constructs and for helpful discussions and advice. We thank Marion H Brown and Omer Dushek and their groups for helpful discussion.

This work was supported by a Wellcome Trust Senior Investigator Award (P.A.v.d.M., grant reference: 101799/Z/13/Z) and a Nuffield Medical Fellowship from the Australian Academy of Science (J.G., grant reference: #1016848).

Author Contributions

The study was conceived by PAvdM and JG, the experiments were performed by MIB with reagents prepared by RLP and EMD, the paper was drafted by MIB and PAvdM and finalized by all authors.

Competing interests

PAvdM is a founder of MatchBio Limited.

557 ## References

558
559

560 Al-Aghbar MA, Chu Y-S, Chen B-M, Roffler SR. 2018. High-Affinity Ligands Can Trigger T Cell Receptor
561 Signaling Without CD45 Segregation. *Frontiers in immunology* **9**:523. doi:10.3389/fimmu.2018.00713

562 Angata T, Hayakawa T, Yamanaka M, Varki A, Nakamura M. 2006. Discovery of Siglec-14, a novel sialic
563 acid receptor undergoing concerted evolution with Siglec-5 in primates. *FASEB J* **20**:1964–1973.
564 doi:10.1096/fj.06-5800com

565 Auwerx J. 1991. The human leukemia cell line, THP-1: A multifacetted model for the study of monocyte-
566 macrophage differentiation. *Experientia* **47**:22–31. doi:10.1007/bf02041244

567 Baggiolini M, Clark-Lewis I. 1992. Interleukin-8, a chemotactic and inflammatory cytokine. *FEBS Lett*
568 **307**:97–101. doi:10.1016/0014-5793(92)80909-z

569 Bakalar MH, Joffe AM, Schmid EM, Son S, Podolski M, Fletcher DA. 2018. Size-Dependent Segregation
570 Controls Macrophage Phagocytosis of Antibody-Opsonized Targets. *Cell* **174**:131–142.
571 doi:10.1016/j.cell.2018.05.059

572 Baqui AAMA, Meiller TF, Falkler WA. 1999. Enhanced interleukin-8 production in THP-1 human
573 monocytic cells by lipopolysaccharide from oral microorganisms and granulocyte-macrophage
574 colony-stimulating factor. *Oral Microbiol Immunol* **14**:275–280. doi:10.1034/j.1399-
575 302x.1999.140502.x

576 Barclay AN, Brown MH, Law SKA, McKnight AJ, Tomlinson MG, Van der Merwe PA. 1997. The Leucocyte
577 Antigen Factsbook, 2nd ed, Academic Press. Academic Press.

578 Boniface JJ, Boniface J, Rabinowitz JD, Rabinowitz J, Wulfing C, Hampl J, Reich Z, Altman J, Altman JD,
579 Kantor RM, Kantor R, Beeson C, McConnell HM, McConnell H, Davis M M, Davis Mark M. 1998.
580 Initiation of signal transduction through the T cell receptor requires the multivalent engagement of
581 peptide/MHC ligands [corrected]. *IMMUNITY* **9**:459–466.

582 Burroughs NJ, Lazic Z, Van der Merwe PA. 2006. Ligand detection and discrimination by spatial
583 relocalization: A kinase-phosphatase segregation model of TCR activation. *Biophysical journal*
584 **91**:1619–1629. doi:10.1529/biophysj.105.080044

585 Chang VT, Fernandes RA, Ganzinger KA, Lee SF, Siebold C, McColl J, Jönsson P, Palayret M, Harlos K,
586 Coles CH, Jones EY, Lui Y, Huang E, Gilbert RJC, Klenerman D, Aricescu AR, Davis SJ. 2016. Initiation of
587 T cell signaling by CD45 segregation at “close contacts.” *Nat Immunol* **17**:574–582.
588 doi:10.1038/ni.3392

589 Chen B-M, Al-Aghbar MA, Lee Chien-Hsin, Chang T-C, Su Y-C, Li Y-C, Chang S-E, Chen C-C, Chung T-H, Liao
590 Y-C, Lee Chau-Hwang, Roffler SR. 2017. The Affinity of Elongated Membrane-Tethered Ligands
591 Determines Potency of T Cell Receptor Triggering. *Front Immunol* **8**:793.
592 doi:10.3389/fimmu.2017.00793

593 Chen KY, Jenkins E, Körbel M, Ponjavic A, Lippert AH, Santos AM, Ashman N, O'Brien-Ball C, McBride J,
594 Klenerman D, Davis SJ. 2021. Trapping or slowing the diffusion of T cell receptors at close contacts
595 initiates T cell signaling. *Proc National Acad Sci* **118**:e2024250118. doi:10.1073/pnas.2024250118

596 Choudhuri K, Wiseman D, Brown MH, Gould K, Van der Merwe PA. 2005. T-cell receptor triggering is
597 critically dependent on the dimensions of its peptide-MHC ligand. *Nature* **436**:578–582.
598 doi:10.1038/nature03843

599 Cochran JR, Cameron TO, Stern LJ. 2000. The Relationship of MHC-Peptide Binding and T Cell Activation
600 Probed Using Chemically Defined MHC Class II Oligomers. *Immunity* **12**:241–250. doi:10.1016/s1074-
601 7613(00)80177-6

602 Cordoba S-P, Choudhuri K, Zhang H, Bridge M, Basat AB, Dustin ML, Van der Merwe PA. 2013. The large
603 ectodomains of CD45 and CD148 regulate their segregation from and inhibition of ligated T-cell
604 receptor. *Blood* **121**:4295–4302. doi:10.1182/blood-2012-07-442251

605 Cornish AL, Freeman S, Forbes G, Ni J, Zhang M, Cepeda M, Gentz R, Augustus M, Carter KC, Crocker PR.
606 1998. Characterization of Siglec-5, a Novel Glycoprotein Expressed on Myeloid Cells Related to CD33.
607 *Blood* **92**:2123–2132. doi:10.1182/blood.v92.6.2123.418k20_2123_2132

608 Crocker PR, Paulson JC, Varki A. 2007. Siglecs and their roles in the immune system. *Nature Reviews*
609 *Immunology* **7**:255–266. doi:10.1038/nri2056

610 Davis SJ, Van der Merwe PA. 2006. The kinetic-segregation model: TCR triggering and beyond. *Nat*
611 *Immunol* **7**:803–809. doi:10.1038/ni1369

612 Davis SJ, Van der Merwe PA. 1996. The structure and ligand interactions of CD2: implications for T-cell
613 function. *Immunol Today* **17**:177–187. doi:10.1016/0167-5699(96)80617-7

614 Denham EM, Barton MI, Black SM, Bridge MJ, Wet B de, Paterson RL, Van der Merwe PA, Goyette J.
615 2019. A generic cell surface ligand system for studying cell–cell recognition. *Plos Biol* **17**:e3000549.
616 doi:10.1371/journal.pbio.3000549

617 Dushek O, Goyette J, Van der Merwe PA. 2012. Non-catalytic tyrosine-phosphorylated receptors.
618 *Immunological Reviews* **250**:258–276. doi:10.1111/imr.12008

619 Ford JW, McVicar DW. 2009. TREM and TREM-like receptors in inflammation and disease. *Current*
620 *opinion in immunology* **21**:38–46. doi:10.1016/j.coi.2009.01.009

621 Göhring J, Kellner F, Schrangl L, Platzer R, Klotzsch E, Stockinger H, Huppa JB, Schütz GJ. 2021. Temporal
622 analysis of T-cell receptor-imposed forces via quantitative single molecule FRET measurements. *Nat*
623 *Commun* **12**:2502. doi:10.1038/s41467-021-22775-z

624 Goodridge HS, Reyes CN, Becker CA, Katsumoto TR, Ma J, Wolf AJ, Bose N, Chan ASH, Magee AS,
625 Danielson ME, Weiss A, Vasilakos JP, Underhill DM. 2011. Activation of the innate immune receptor
626 Dectin-1 upon formation of a 'phagocytic synapse.' *Nature* **472**:471–475. doi:10.1038/nature10071

627 Goyette J, Nieves DJ, Ma Y, Gaus K. 2019. How does T cell receptor clustering impact on signal
628 transduction? *Journal of cell science* **132**:jcs226423. doi:10.1242/jcs.226423

629 Jacobson K, Liu P, Lagerholm BC. 2019. The Lateral Organization and Mobility of Plasma Membrane
630 Components. *Cell* **177**:806–819. doi:10.1016/j.cell.2019.04.018

631 James JR, Vale RD. 2012. Biophysical mechanism of T-cell receptor triggering in a reconstituted system.
632 *Nature* **487**:64–69. doi:10.1038/nature11220

633 Jenkins E, Körbel M, O'Brien-Ball C, McColl J, Chen KY, Kotowski M, Humphrey J, Lippert AH, Brouwer H,
634 Santos AM, Lee SF, Davis SJ, Klenerman D. 2023. Antigen discrimination by T cells relies on size-
635 constrained microvillar contact. *Nat Commun* **14**:1611. doi:10.1038/s41467-023-36855-9

636 June CH, Sadelain M. 2018. Chimeric Antigen Receptor Therapy. *New Engl J Med* **379**:64–73.
637 doi:10.1056/nejmra1706169

638 Jung Y, Wen L, Altman A, Ley K. 2021. CD45 pre-exclusion from the tips of T cell microvilli prior to
639 antigen recognition. *Nat Commun* **12**:3872. doi:10.1038/s41467-021-23792-8

640 Köhler K, Xiong S, Brzostek J, Mehrabi M, Eissmann P, Harrison A, Cordoba S-P, Oddos S, Miloserdov V,
641 Gould K, Burroughs NJ, Van der Merwe PA, Davis DM. 2010. Matched sizes of activating and
642 inhibitory receptor/ligand pairs are required for optimal signal integration by human natural killer
643 cells. *PLOS One* **5**:e15374. doi:10.1371/journal.pone.0015374

644 Kusumi A, Suzuki KGN, Kasai RS, Ritchie K, Fujiwara TK. 2011. Hierarchical mesoscale domain
645 organization of the plasma membrane. *Trends in biochemical sciences* **36**:604–615.
646 doi:10.1016/j.tibs.2011.08.001

647 Labanieh L, Mackall CL. 2023. CAR immune cells: design principles, resistance and the next generation.
648 *Nature* **614**:635–648. doi:10.1038/s41586-023-05707-3

649 Lanier LL. 2008. DAP10- and DAP12-associated receptors in innate immunity. *Immunological reviews*
650 **227**:150–160. doi:10.1111/j.1600-065x.2008.00720.x

651 Li Y-C, Chen B-M, Wu P-C, Cheng T-L, Kao L-S, Tao M-H, Lieber A, Roffler SR. 2010. Cutting Edge:
652 Mechanical Forces Acting on T Cells Immobilized via the TCR Complex Can Trigger TCR Signaling. *J*
653 *Immunol* **184**:5959–5963. doi:10.4049/jimmunol.0900775

654 Lim H-S, Cordoba S-P, Dushek O, Goyette J, Taylor A, Rudd CE, Van der Merwe PA. 2015. Costimulation
655 of IL-2 Production through CD28 Is Dependent on the Size of Its Ligand. *J Immunol* **195**:5432–5439.
656 doi:10.4049/jimmunol.1500707

657 Locksley RM, Killeen N, Lenardo MJ. 2001. The TNF and TNF Receptor Superfamilies Integrating
658 Mammalian Biology. *Cell* **104**:487–501. doi:10.1016/s0092-8674(01)00237-9

659 Ma Z, Janmey PA, Finkel TH. 2008. The receptor deformation model of TCR triggering. *The FASEB Journal*
660 **22**:1002–1008. doi:10.1096/fj.07-9331hyp

661 Van der Merwe PA, Barclay AN. 1994. Transient intercellular adhesion: the importance of weak protein-
662 protein interactions. *Trends Biochem Sci* **19**:354–358. doi:10.1016/0968-0004(94)90109-0

663 Van der Merwe PA, Davis SJ, Shaw AS, Dustin ML. 2000. Cytoskeletal polarization and redistribution of
664 cell-surface molecules during T cell antigen recognition. *Semin Immunol* **12**:5–21.
665 doi:10.1006/smim.2000.0203

666 Milstein O, Tseng S-Y, Starr T, Llodra J, Nans A, Liu M, Wild MK, Van der Merwe PA, Stokes DL, Reisner Y,
667 Dustin ML. 2008. Nanoscale Increases in CD2-CD48-mediated Intermembrane Spacing Decrease
668 Adhesion and Reorganize the Immunological Synapse*. *J Biol Chem* **283**:34414–34422.
669 doi:10.1074/jbc.m804756200

670 O'Shea JJ, McVicar DW, Bailey TL, Burns C, Smyth MJ. 1992. Activation of human peripheral blood T
671 lymphocytes by pharmacological induction of protein-tyrosine phosphorylation. *Proceedings of the*
672 *National Academy of Sciences of the United States of America* **89**:10306–10310.

673 Parodi M, Favoreel H, Candiano G, Gaggero S, Sivori S, Mingari MC, Moretta L, Vitale M, Cantoni C. 2019.
674 NKp44-NKp44 Ligand Interactions in the Regulation of Natural Killer Cells and Other Innate Lymphoid
675 Cells in Humans. *Front Immunol* **10**:719. doi:10.3389/fimmu.2019.00719

676 Patel A, Andre V, Eguiguren SB, Barton MI, Denham EM, Pettmann J, Morch AM, Kutuzov M, Siller-Farfan
677 JA, Dustin ML, Van der Merwe PA, Dushek O. 2023. Using CombiCells, a platform enabling titration
678 and combinatorial display of cell surface ligands, to investigate the sensitivity and costimulatory
679 requirements of TCRs and CARs. doi:10.1101/2023.06.15.545075

680 Razvag Y, Neve-Oz Y, Sajman J, Reches M, Sherman E. 2018. Nanoscale kinetic segregation of TCR and
681 CD45 in engaged microvilli facilitates early T cell activation. *Nature Communications* **9**:732.
682 doi:10.1038/s41467-018-03127-w

683 Sadelain M. 2016. Chimeric antigen receptors: driving immunology towards synthetic biology. *Current*
684 *opinion in immunology* **41**:68–76. doi:10.1016/j.coi.2016.06.004

685 Schamel WW, Alarcón B, Minguet S. 2019. The TCR is an allosterically regulated macromolecular
686 machinery changing its conformation while working. *Immunological reviews* **291**:8–25.
687 doi:10.1111/imr.12788

688 Schmid EM, Bakalar MH, Choudhuri K, Weichsel J, Ann HS, Geissler PL, Dustin ML, Fletcher DA. 2016.
689 Size-dependent protein segregation at membrane interfaces. *Nat Phys* **12**:704–711.
690 doi:10.1038/nphys3678

691 Secrist JP, Burns LA, Karnitz L, Koretzky GA, Abraham RT. 1993. Stimulatory effects of the protein
692 tyrosine phosphatase inhibitor, pervanadate, on T-cell activation events. *Journal of Biological*
693 *Chemistry* **268**:5886–5893.

694 Sharma P, Allison JP. 2015. The future of immune checkpoint therapy. *Science* **348**:56–61.
695 doi:10.1126/science.aaa8172

696 Shilts J, Severin Y, Galaway F, Müller-Sienerth N, Chong Z-S, Pritchard S, Teichmann S, Vento-Tormo R,
697 Snijder B, Wright GJ. 2022. A physical wiring diagram for the human immune system. *Nature*
698 **608**:397–404. doi:10.1038/s41586-022-05028-x

699 Springer TA. 1990. Adhesion receptors of the immune system. *Nature* **346**:425–434.
700 doi:10.1038/346425a0

701 Stinchcombe JC, Asano Y, Kaufman CJG, Böhlig K, Peddie CJ, Collinson LM, Nadler A, Griffiths GM. 2023.
702 Ectocytosis renders T cell receptor signaling self-limiting at the immune synapse. *Science* **380**:818–
703 823. doi:10.1126/science.abp8933

704 Ullrich A, Schlessinger J. 1990. Signal transduction by receptors with tyrosine kinase activity. *Cell*
705 **61**:203–212. doi:10.1016/0092-8674(90)90801-k

706 Varma R, Campi G, Yokosuka T, Saito T, Dustin ML. 2006. T Cell Receptor-Proximal Signals Are Sustained
707 in Peripheral Microclusters and Terminated in the Central Supramolecular Activation Cluster.
708 *Immunity* **25**:117–127. doi:10.1016/j.immuni.2006.04.010

709 Wild MK, Cambiaggi A, Brown MH, Davies EA, Ohno H, Saito T, Van der Merwe PA. 1999. Dependence of
710 T Cell Antigen Recognition on the Dimensions of an Accessory Receptor–Ligand Complex. *J Exp*
711 *Medicine* **190**:31–42. doi:10.1084/jem.190.1.31

712 Wilhelm KB, Morita S, McAffee DB, Kim S, O'Dair MK, Groves JT. 2021. Height, but not binding epitope,
713 affects the potency of synthetic TCR agonists. *Biophys J* **120**:3869–3880.
714 doi:10.1016/j.bpj.2021.08.027

715 Wu H, Kwong PD, Hendrickson WA. 1997. Dimeric association and segmental variability in the structure
716 of human CD4. *Nature* **387**:527–530. doi:10.1038/387527a0

717 Xiao Q, Zhang X, Tu L, Cao J, Hinrichs CS, Su X. 2022. Size-dependent activation of CAR-T cells. *Sci*
718 *Immunol* **7**:eabl3995. doi:10.1126/sciimmunol.abl3995

719 Zhu C, Chen W, Lou J, Rittase W, Li K. 2019. Mechanosensing through immunoreceptors. *Nat Immunol*
720 **20**:1269–1278. doi:10.1038/s41590-019-0491-1

721

722 ## Figure legends

723 **Figure 1 Testing the effect of increasing ligand length on NTR activation**

724 (A) Schematic depiction of the components of the generic ligand system used to test the effect of
725 increasing ligand length and valency. The shared DAP-12 signalling homodimer is grey. With tetravalent
726 streptactin (not shown) all four of the binding sites are able to bind Steptag II (B) Representative flow
727 cytometry data from a conjugation assay between SIRPβ1 expressing THP1 receptor cells and CHO cells
728 expressing short ligands coupled with the indicated concentration of monovalent Strep-Tactin
729 SpyCatcher. Receptor and ligand cells were stained with CellTrace Violet and Far Red, respectively, and
730 events in the upper right quadrant were presumed to be conjugates. (C) Conjugation of (left panel) and
731 IL-8 secretion by (middle panel) SIRPβ1 expressing THP1 cells incubated with CHO cells expressing the
732 indicated number of short (blue) or long (red) monovalent ligands, measured as described in the
733 Materials and Methods using parameters determined in sFigure 1. IL-8 secretion is plotted against
734 conjugation in the right panel. These are representative results from three independent experiments,
735 which are combined in Figure 2A for statistical analysis. Due to experimental constraints the stimulation
736 and conjugation assays in this (and subsequent) experiment(s) were performed on successive days. The
737 same result was obtained when performed on the same day (sFigure 2).

738 **Figure 2: The effect of NTR ligand length on activation via four NTRs.**

739 THP-1 cells expressing (A) SIRPβ1, (B) Siglec 14, (C) NKp44 or (D) TREM-1 with N-terminal StrepTagII
740 peptides were incubated with CHO cells expressing the indicated numbers of short (blue) or long (red)
741 monovalent generic ligand binding sites and conjugate formation (left panel) and IL-8 release (middle
742 panel) measured. Ligand binding sites were determined as described in the Materials and Methods
743 using parameters determined in sFigure 1. The IL-8 release versus conjugation level is plotted in the
744 right panels. The data from three biological replicates (including one SIRPβ1 replicate shown in Figure 1)
745 are plotted with the data normalised to the level of conjugation or stimulation achieved with the short
746 ligand within each replicate. The data were fitted as described in the Materials and Methods and an F
747 test was used to test the significance of differences between the fits.

748 **Figure 3: Effect of ligand anchor on SIRPβ1 stimulation**

749 (A) Schematic depiction of the components of the generic ligand system used to test the effect of
750 varying the ligand anchor. (B) The diffusion coefficients of the different ligand anchors were measured
751 by FRAP after coupling GFP-Spycatcher. The mean and SD from three independent experiments were
752 compared by ANOVA. (C) THP-1 cells expressing SIRPβ1 with an N-terminal StrepTagII peptide were
753 incubated with CHO cells expressing the indicated number of ligand binding sites with CD80 (blue), CD43

754 (orange) or CD52 (green) anchors, and conjugate formation (left panel) and IL-8 release (right panel)
755 measured. Ligand binding sites were determined as described in the Materials and Methods using
756 parameters determined in sFigure 4. The IL-8 release versus conjugation level is plotted in the right
757 panel. The data from three biological replicates are plotted with the data normalised to the level of
758 conjugation or stimulation achieved with the CD52 ligand anchor within each replicate. These data were
759 fitted as described in the Materials and Methods and an F test was used to test the significance of
760 differences between the fits collectively and pairwise (Tables).

761 **Figure 4: Effect of ligand valency on NTR stimulation.**

762 THP-1 cells expressing (A) SIRPβ1, (B) Siglec 14, (C) NKp44 or (D) TREM-1 with N-terminal StrepTagII
763 peptides were incubated with CHO cells expressing the indicated numbers of monovalent (filled circles)
764 or tetravalent (open circles) short generic ligand binding sites and conjugate formation (left panel) and
765 IL-8 release (middle panel) measured. Ligand binding sites were determined as described in the
766 Materials and Methods using parameters determined in sFigure 6. The IL-8 release versus conjugation
767 level is plotted in the right panels. The data from three biological replicates are plotted with the data
768 normalised to the level of conjugation or stimulation achieved with the short tetravalent ligand within
769 each replicate. These data were fitted as described in the Materials and Methods and an F test was used
770 to test the significance of differences between the fits.

771 **Figure 5: The effect of NTR ligand length on activation by tetravalent ligands**

772 THP-1 cells expressing (A) SIRPβ1, (B) Siglec 14, (C) NKp44 or (D) TREM-1 with N-terminal StrepTagII
773 peptides were incubated with CHO cells expressing the indicated numbers of short (blue) or long (red)
774 tetravalent ligand binding sites and conjugate formation (left panel) and IL-8 release (middle panel)
775 measured. Ligand binding sites were determined as described in the Materials and Methods using
776 parameters determined in sFigure 9. The IL-8 release versus conjugation level is plotted in the right
777 panels. The data from three biological replicates are plotted with the data normalised to the level of
778 conjugation or stimulation achieved with the short tetravalent ligand within each replicate. These data
779 were fitted as described in the Materials and Methods and an F test was used to test the significance of
780 differences between the fits.

781

782 ## Supplementay Figure legends

783 **sFigure 1. Measuring the K_D and maximum number of binding sites on CHO cell expressing short and**
784 **long CD80 ligand anchors**

785 (A) Short (blue) or long (red) CD80 ligand CHO cells were incubated with the indicated concentration of
786 monovalent StrepTactin SpyCatcher before labelling with biotin Atto 488 followed by flow cytometry. A
787 one site simple binding model was fitted to the data (lines) to determine the K_D. (B) The mean and SD of
788 K_D values from six independent experiments were compared using a t test. (C) Short or long CD80 ligand
789 CHO cells or control (empty, grey) CHO cells were incubated with a saturating concentration (15 µM) of
790 monovalent StrepTactin SpyCatcher before mixing with the indicated concentration of biotin-4-
791 fluorescein and the unquenched fluorescence in the media measured after binding. (D) The mean and
792 SD of the maximum number of binding sites per cell from six independent experiments were compared
793 using a t test.

794 **sFigure 2. Testing the effect of increasing ligand length on NTR activation**

795 Repeat of experiment Figure 1 with both conjugation and stimulation assays performed on the same day
796 with the same cells split. THP-1 cells expressing SIRPβ1 were incubated with CHO cells expressing the
797 indicated numbers of short (blue) or long (red) generic ligand binding sites and conjugate formation (A)
798 and IL-8 release (B) measured. Ligand binding sites were determined as described in the Materials and
799 Methods using parameters determined in sFigure 1. The IL-8 release versus conjugation level is plotted
800 in (C).

801 **sFigure 3. The effect of NTR length on activation.**

802 The data from Figure 2 has been reanalysed to enable comparison between NTRs. THP-1 cells expressing
803 the indicated NTR with N-terminal StrepTagII peptides were incubated with CHO cells expressing the
804 indicated numbers of short (A) or long (B) generic ligand binding sites and conjugate formation (left
805 panel) and IL-8 release (middle panel) measured. The IL-8 release versus conjugation level is plotted in
806 the right panels. The data were fitted as described in the Materials and Methods and an F test was used
807 to test the significance of differences between the fits collectively (panels) and pairwise (corresponding
808 Tables).

809 **sFigure 4. Measuring mobility, K_D and the maximum generic binding sites on CHO cell expressing**
810 **different ligand anchors**

811 (A) CHO cells expression with the indicated generic ligand anchor were labelled with SpyCatcher-GFP
812 and fluorescent recovery after 20 s photobleaching (FRAP) was performed. The recovery half-times,
813 which were used to calculate diffusion coefficients, were determined from fits (lines) to the data

814 (circles). (B) Mean and SD of K_D values determined as in sFigure 1 from nine independent experiments
815 (C) Mean and SD of maximum number of binding sites determined as in sFigures 1 from six independent
816 experiments. To enable comparison to monovalent sites the tetravalent values divided by four, labelled
817 (/4), were also plotted.

818 **sFigure 5. Turnover of ligand anchor at the cell surface.**

819 (A-C) Monovalent StrepTactin SpyCatcher was coupled to CHO cells expressing the indicated ligand
820 anchor and cells incubated at 37 C for the indicated times. Cells were stained with biotin ATTO 488 and
821 analysed by flow cytometry to assess the level of the cell surface StrepTactin. The graphs show the
822 relative level of ligand expression with the maximum normalised to time zero. The data is a
823 representative of three biological replicates and was fit with an exponential one phase decay model. (D)
824 The mean and SD of the half-time for loss from the cell surface for three biological replicates were
825 compared by ANOVA.

826 **sFigure 6. Measuring the K_D and maximum number of binding sites on CHO cell presenting**
827 **monovalent or tetravalent StrepTactin SpyCatcher**

828 (A) Short CD80 ligand CHO cells were incubated with the indicated concentration of monovalent (closed
829 circles) or tetravalent (open circles) StrepTactin SpyCatcher before labelling with biotin Atto 488
830 followed by flow cytometry. A one site simple binding model was fitted to the data (lines) to determine
831 the K_D. (B) The mean and SD of K_D values from eight independent experiments were compared using a t
832 test. (C) Short CD80 ligand CHO cells or control (empty, grey) CHO cells were incubated with a saturating
833 concentration monovalent (10 µM) or tetravalent (10 µM) StrepTactin SpyCatcher before mixing with
834 the indicated concentration of biotin-4-fluorescein and the unquenched florescence in the media
835 measured after binding. (D) The mean and SD of the maximum number of binding sites per cell from five
836 independent experiments were compared by ANOVA. To enable comparison to monovalent sites the
837 tetravalent values divided by four were also plotted.

838 **sFigure 7. Effect of anchor on NTR stimulation by multivalent ligand**

839 THP-1 cells expressing (A) SIRPβ1, (B) Siglec 14, (C) NKp44 or (D) TREM-1 with an N-terminal StrepTagII
840 peptide were incubated with CHO cells expressing the indicated number of monovalent (closed circles)
841 or multivalent (open circles) ligand binding sites with the indicated ligand anchors and IL-8 release
842 measured. Ligand binding sites were determined as described in the Materials and Methods using
843 parameters determined in sFigure 4. The data from three biological replicates are plotted with the data
844 normalised to the level of stimulation achieved with the CD80 ligand coupled with tetravalent ligand

845 within each replicate. These data were fitted as described in the Material and Methods and an F test
846 was used to test the significance of differences between the fits collectively and pairwise (Tables).

847 **sFigure 8. Effect of anchor on SIRPβ1 stimulation by multivalent ligand**

848 THP-1 cells expressing SIRPβ1 with an N-terminal StrepTagII peptide were incubated with CHO cells
849 expressing the indicated number of ligand binding sites presented on monovalent (closed circles) or
850 multivalent (open circles) ligand and conjugate formation (left panel) and IL-8 release (middle panel)
851 were measured. Ligand binding sites were determined as described in the Materials and Methods using
852 parameters determined in sFigure 4. The IL-8 release versus conjugation level is plotted in the right
853 panel. The data from three biological replicates are plotted with the data normalised to the level of
854 conjugation or stimulation achieved with the tetravalent ligand within each replicate. These data were
855 fitted as described in the Material and Methods and an F test was used to test the significance of
856 differences between the fits.

857 **sFigure 9. Measuring the K_D and maximum number of binding sites on CHO cell presenting tetravalent**
858 **StrepTactin SpyCatcher coupled to short versus long ligand anchors**

859 (A) Short (blue) or long (red) CD80 ligand CHO cells were incubated with the indicated concentration of
860 tetravalent StrepTactin SpyCatcher before labelling with biotin Atto 488 followed by flow cytometry. A
861 one site simple binding model was fitted to the data (lines) to determine the K_D. (B) The mean and SD of
862 K_D values from six independent experiments were compared using a t test. (C) Short or long CD80 ligand
863 CHO cells or control (empty, grey) CHO cells were incubated with a saturating concentration (10 µM) of
864 tetravalent StrepTactin SpyCatcher before mixing with the indicated concentration of biotin-4-
865 fluorescein and the unquenched florescence in the media measured after binding. (D) The mean and SD
866 of the maximum number of binding sites per cell from six independent experiments were compared
867 using a t test.

868

Figure 1

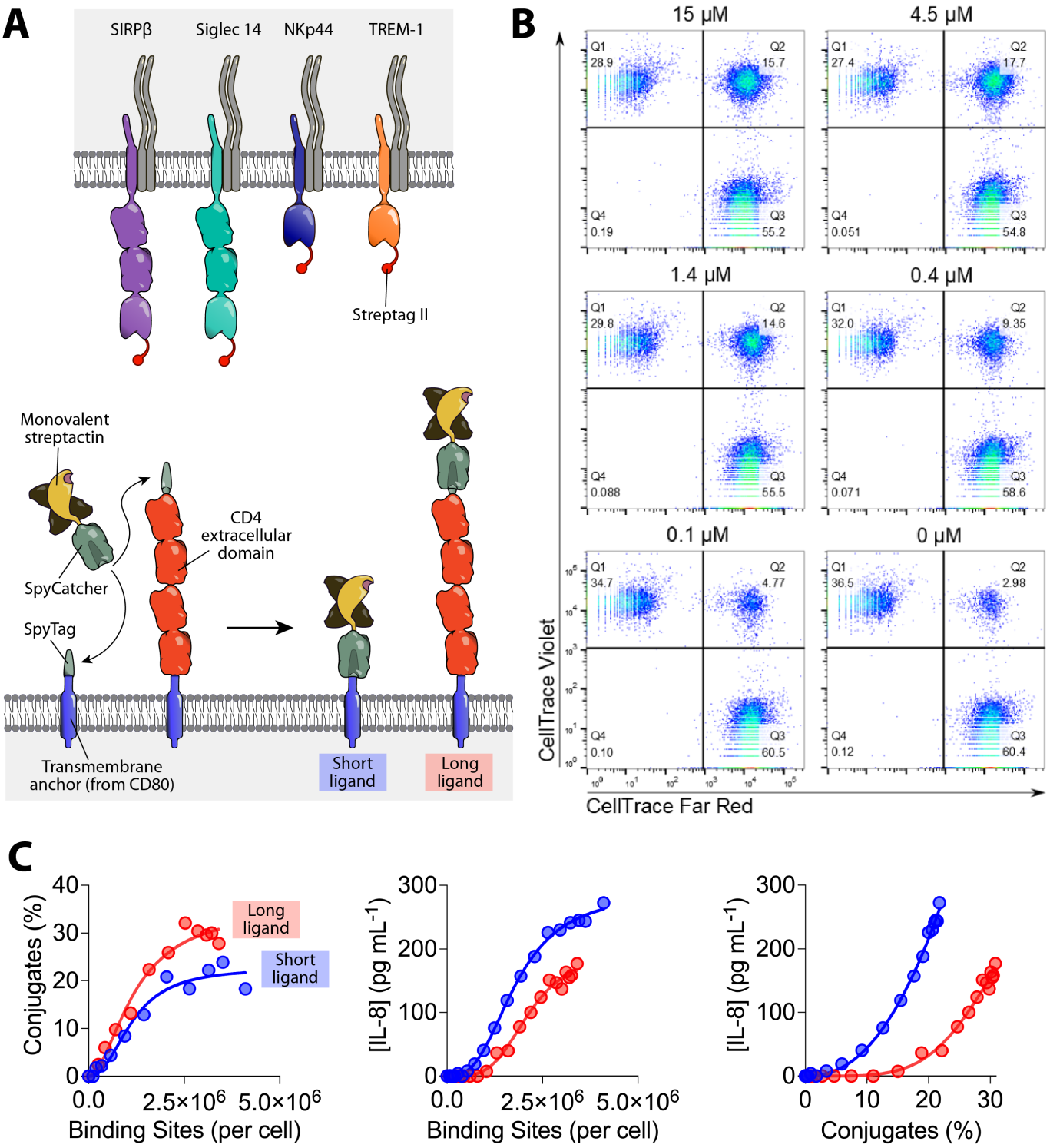
A
SIRPβ
Siglec 14
NKp44
TREM-1
Streptag II
Monovalent streptactin
SpyCatcher
SpyTag
CD4 extracellular domain
Transmembrane anchor (from CD80)
Short ligand
Long ligand
B
15 μM
4.5 μM
1.4 μM
0.4 μM
0.1 μM
0 μM
CellTrace Violet
CellTrace Far Red
C
Conjugates (%)
Binding Sites (per cell)
[IL-8] (pg mL-1)
Long ligand
Short ligand

Figure 2

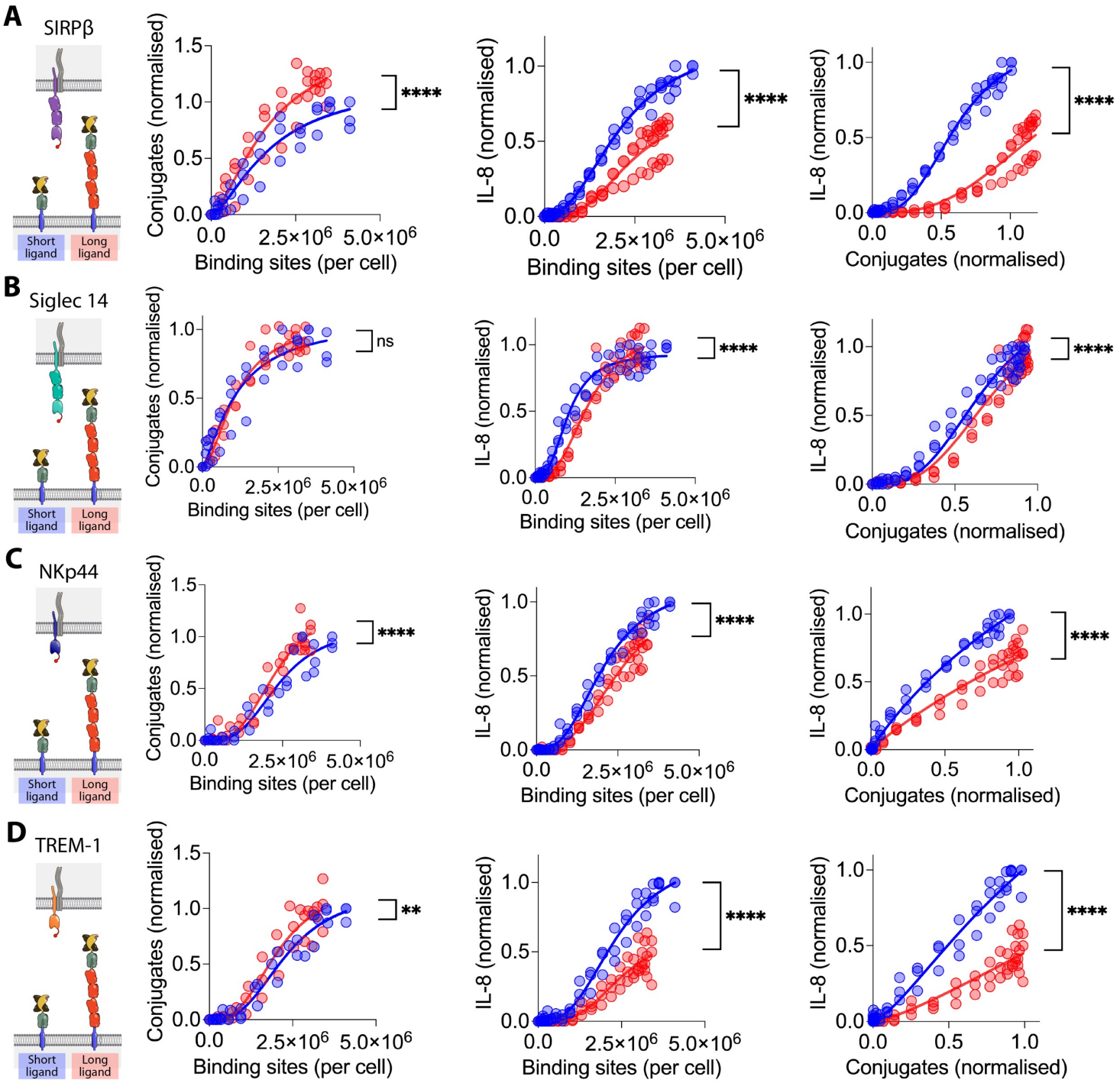
A
SIRPβ
Short ligand
Long ligand
Conjugates (normalised)
Binding sites (per cell)
IL-8 (normalised)
Conjugates (normalised)
****
B
Siglec 14
ns
C
NKp44
D
TREM-1
**

Figure 3

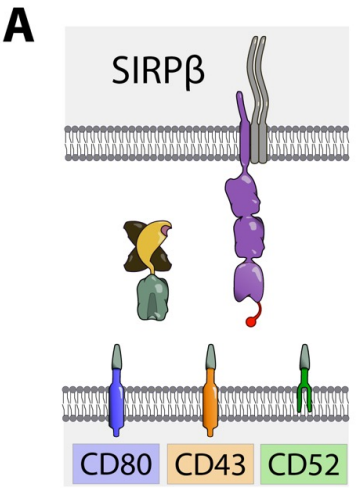

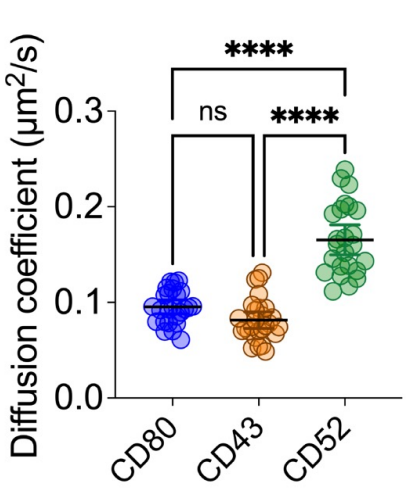

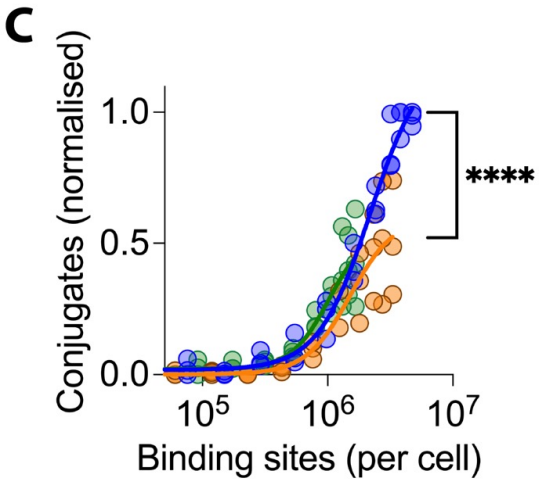

Pairwise F-test p values

	CD43	CD52
CD80	<0.0001	0.510
CD43		0.114

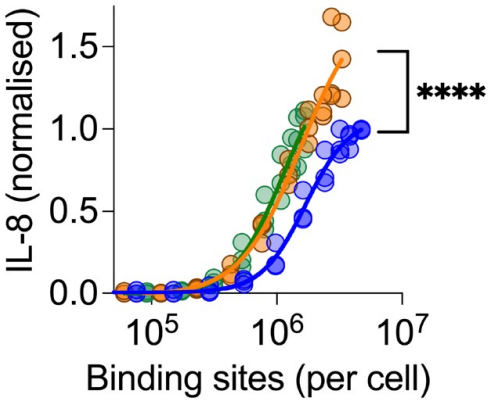

Pairwise F-test p values

	CD43	CD52
CD80	<0.0001	<0.0001
CD43		0.432

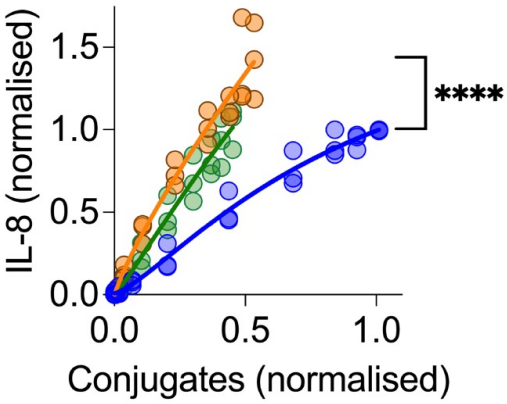

Pairwise F-test p values

	CD43	CD52
CD80	<0.0001	<0.0001
CD43		<0.0001

Figure 4

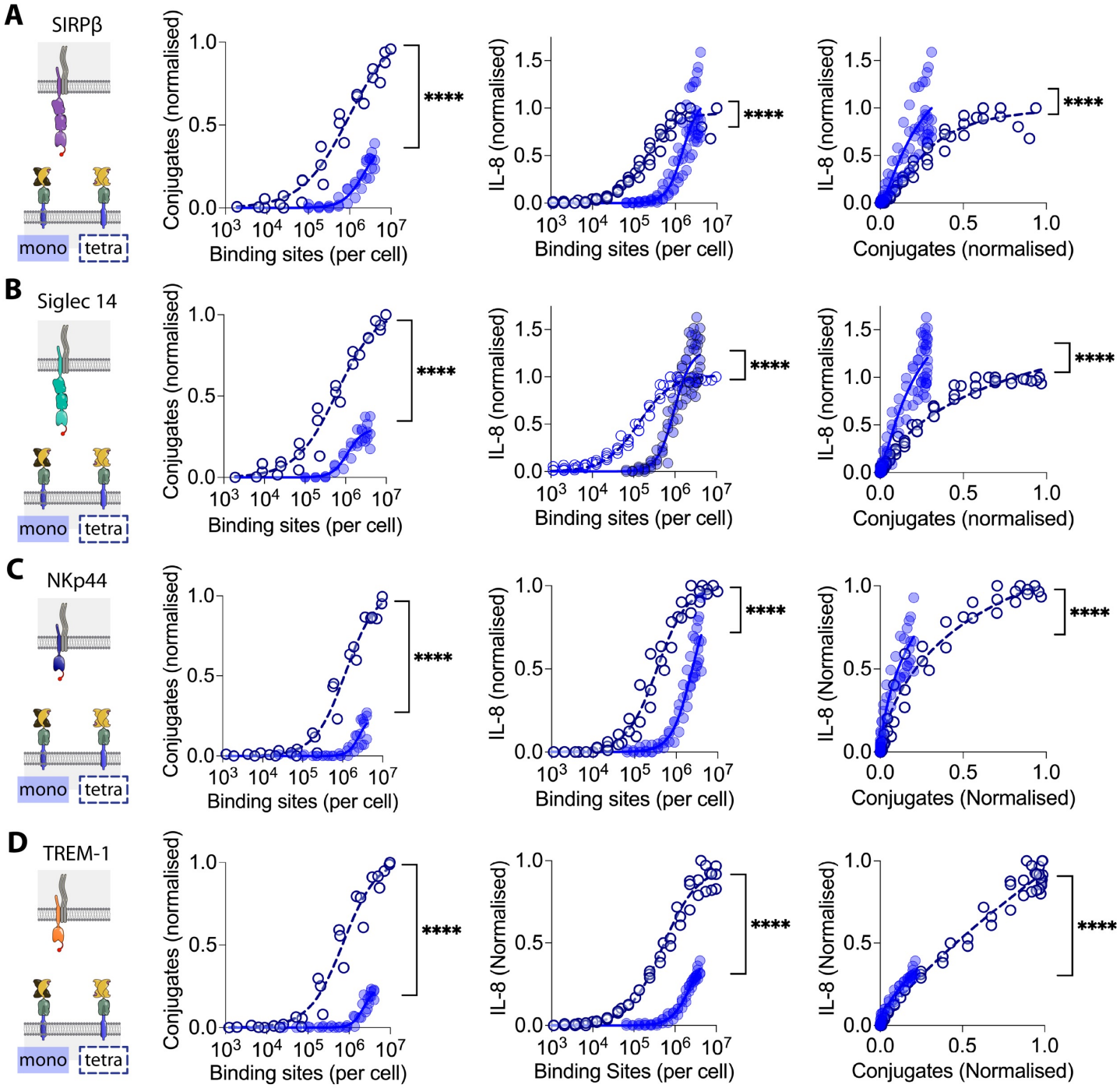
A
SIRPβ
mono
tetra
Conjugates (normalised)
Binding sites (per cell)
IL-8 (normalised)
Conjugates (normalised)
****
B
Siglec 14
C
NKp44
IL-8 (Normalised)
Conjugates (Normalised)
D
TREM-1
Binding Sites (per cell)

Figure 5

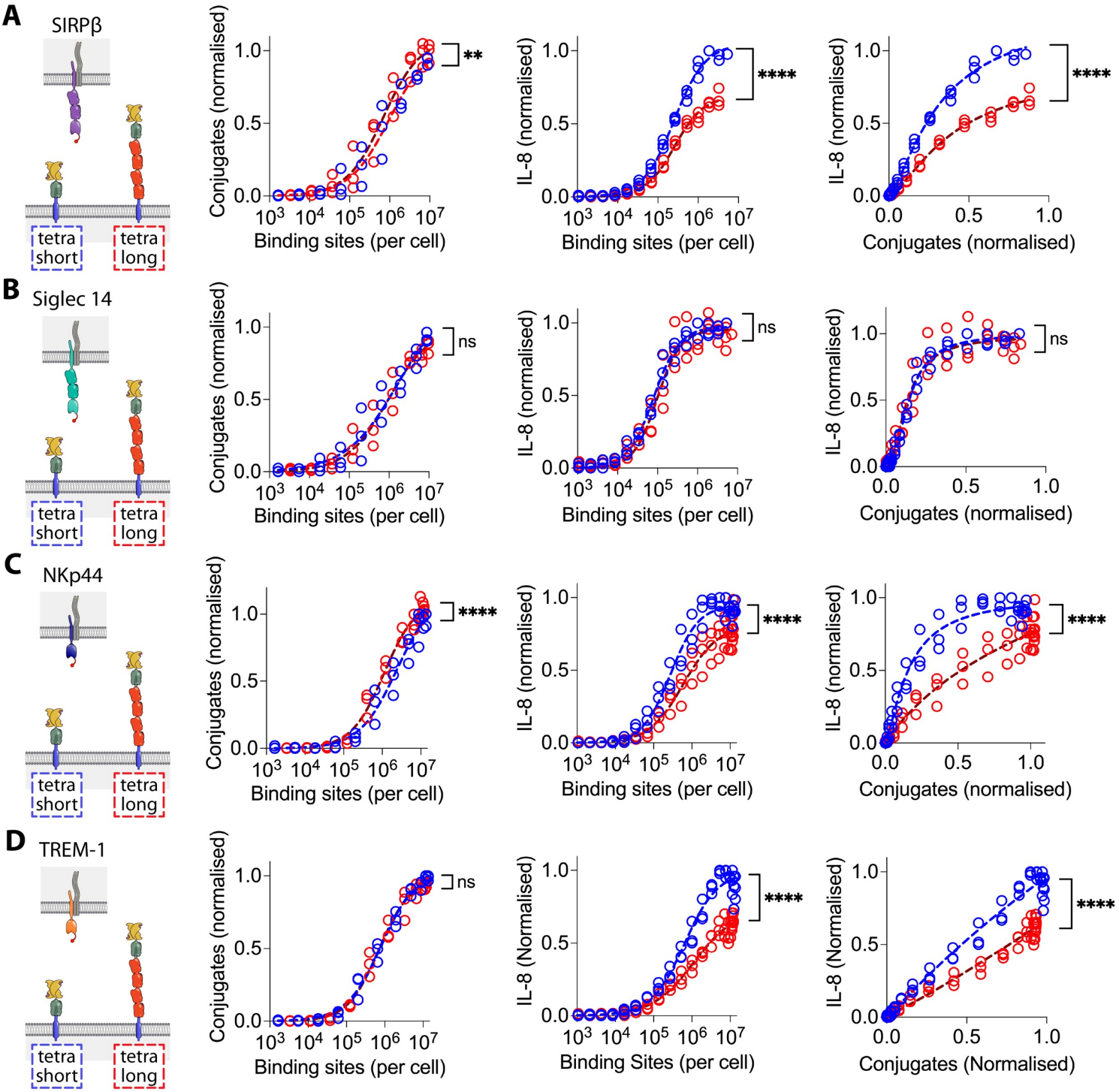
A
SIRPβ
tetra short
tetra long
Conjugates (normalised)
Binding sites (per cell)
**
IL-8 (normalised)
Binding sites (per cell)
****
IL-8 (normalised)
Conjugates (normalised)
****
B
Siglec 14
tetra short
tetra long
Conjugates (normalised)
Binding sites (per cell)
ns
IL-8 (normalised)
Binding sites (per cell)
ns
IL-8 (normalised)
Conjugates (normalised)
ns
C
NKp44
tetra short
tetra long
Conjugates (normalised)
Binding sites (per cell)
****
IL-8 (normalised)
Binding sites (per cell)
****
IL-8 (normalised)
Conjugates (normalised)
****
D
TREM-1
tetra short
tetra long
Conjugates (normalised)
Binding sites (per cell)
ns
IL-8 (Normalised)
Binding Sites (per cell)
****
IL-8 (Normalised)
Conjugates (Normalised)
****

sFigure 1

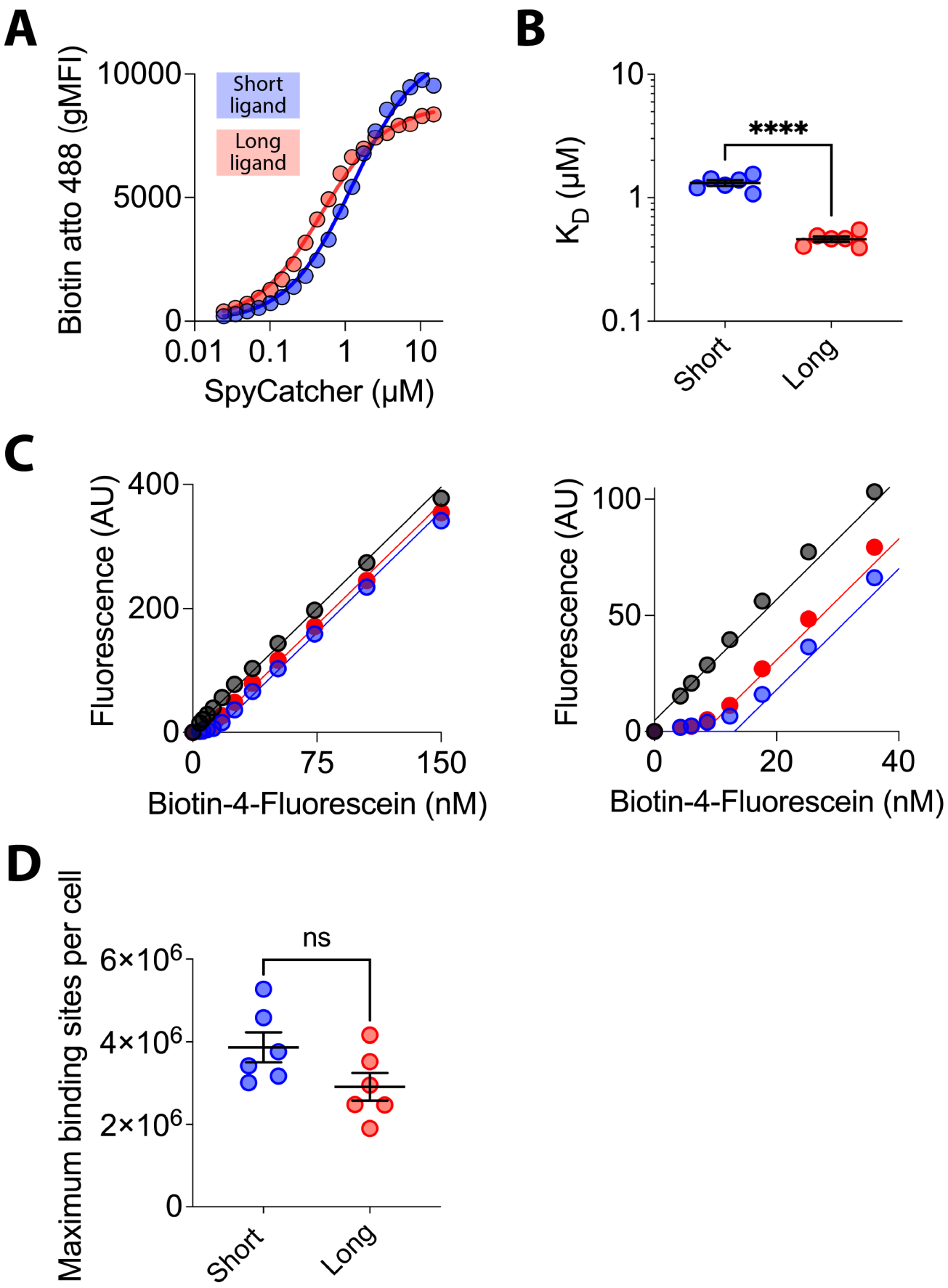
A
Biotin atto 488 (gMFI)
10000
5000
0
Short ligand
Long ligand
0.01
0.1
1
10
SpyCatcher (μM)
B
K_D (μM)
10
1
0.1
****
Short
Long
C
Fluorescence (AU)
400
200
0
0
75
150
Biotin-4-Fluorescein (nM)
Fluorescence (AU)
100
50
0
0
20
40
Biotin-4-Fluorescein (nM)
D
Maximum binding sites per cell
6×10^6
4×10^6
2×10^6
0
ns
Short
Long

sFigure 2

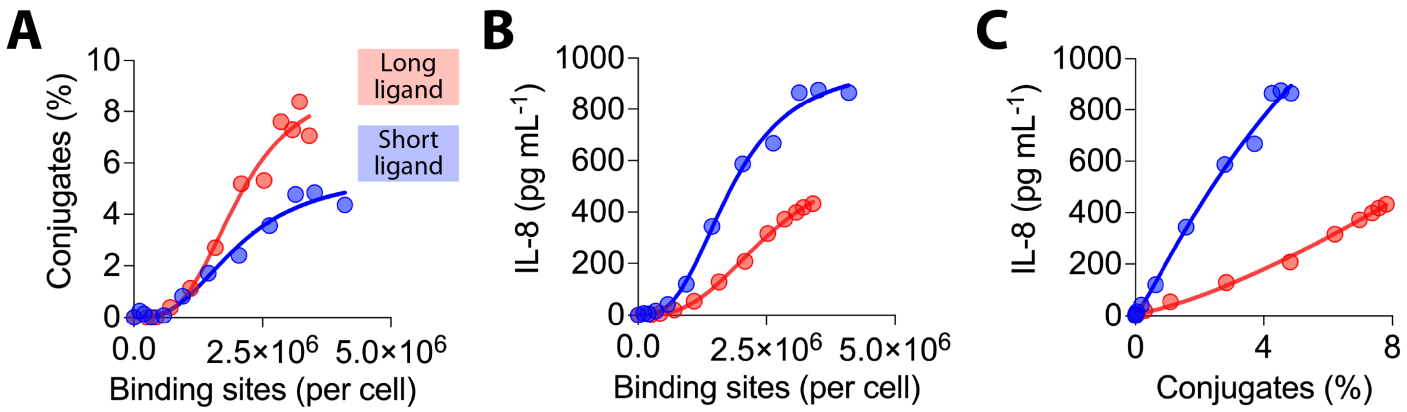
A
Conjugates (%)
10
8
6
4
2
0
0.0
2.5×10^6
5.0×10^6
Binding sites (per cell)
Long ligand
Short ligand
B
IL-8 (pg mL^-1)
1000
800
600
400
200
0
0.0
2.5×10^6
5.0×10^6
Binding sites (per cell)
C
IL-8 (pg mL^-1)
1000
800
600
400
200
0
0
4
8
Conjugates (%)

sFigure 3

A

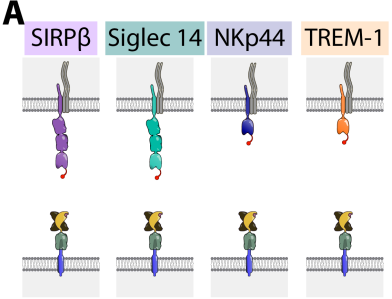

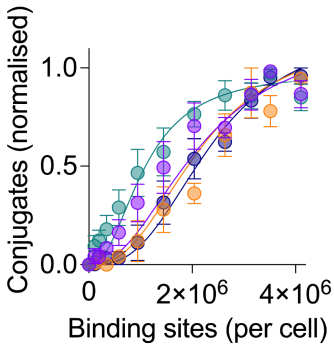

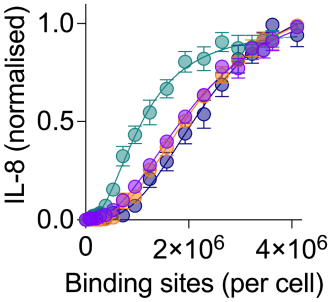

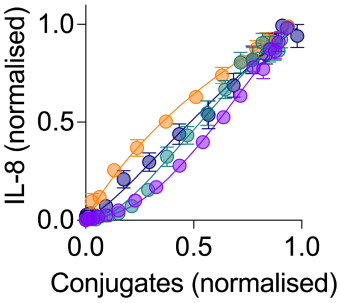

Pairwise F-test p values

	Siglec 14	NKp44	TREM-1
SIRPβ	0.0443	<0.0001	<0.0001
Siglec 14		<0.0001	<0.0001
NKp44			0.404

Pairwise F-test p values

	Siglec 14	NKp44	TREM-1
SIRPβ	<0.0001	0.0699	<0.0001
Siglec 14		<0.0001	<0.0001
NKp44			0.0055

Pairwise F-test p values

	Siglec 14	NKp44	TREM-1
SIRPβ	<0.0001	<0.0001	<0.0001
Siglec 14		<0.0001	<0.0001
NKp44			<0.0001

B

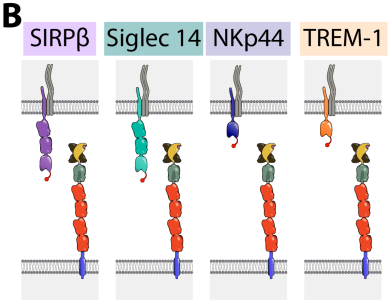

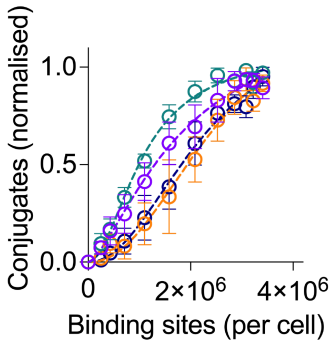

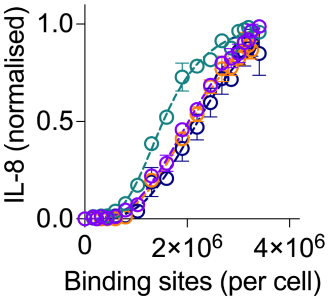

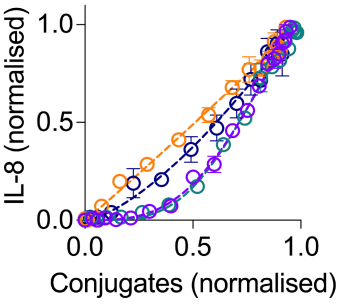

Pairwise F-test p values

	Siglec 14	NKp44	TREM-1
SIRPβ	0.0084	<0.0001	<0.0001
Siglec 14		<0.0001	<0.0001
NKp44			0.5775

Pairwise F-test p values

	Siglec 14	NKp44	TREM-1
SIRPβ	<0.0001	0.0873	<0.0001
Siglec 14		<0.0001	<0.0001
NKp44			0.0467

Pairwise F-test p values

	Siglec 14	NKp44	TREM-1
SIRPβ	0.0036	<0.0001	<0.0001
Siglec 14		<0.0001	<0.0001
NKp44			0.0004

sFigure 4

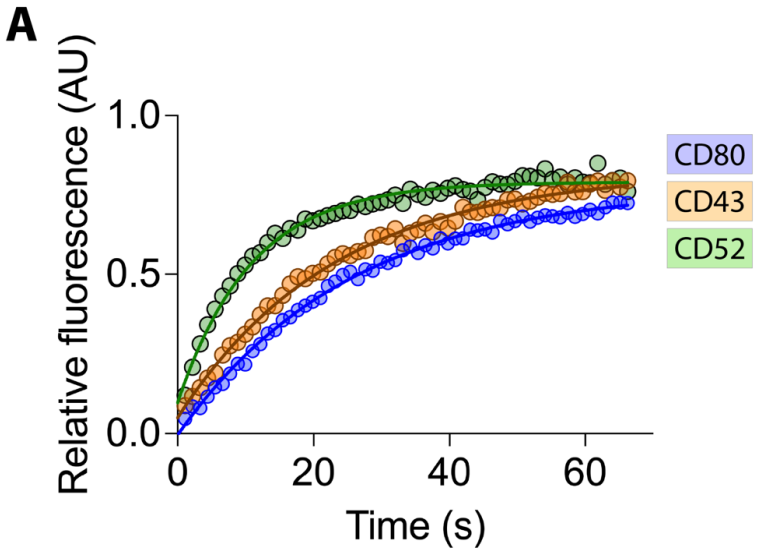
A
Relative fluorescence (AU)
1.0
0.5
0.0
0
20
40
60
Time (s)
CD80
CD43
CD52

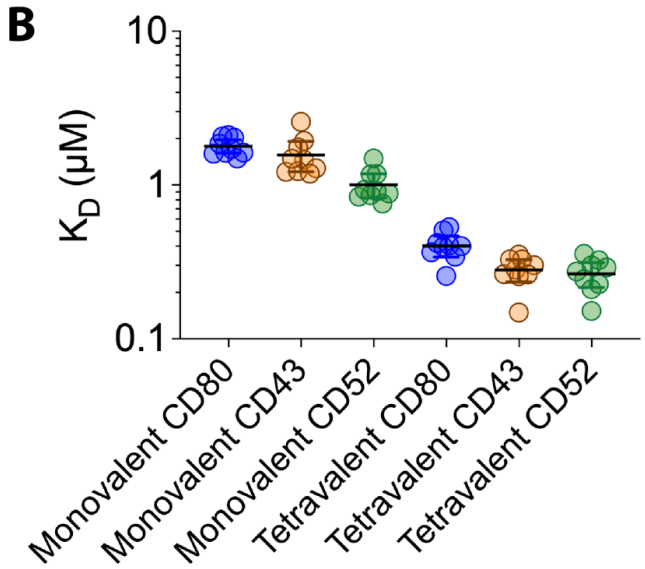
B
K_D (μM)
10
1
0.1
Monovalent CD80
Monovalent CD43
Monovalent CD52
Tetravalent CD80
Tetravalent CD43
Tetravalent CD52

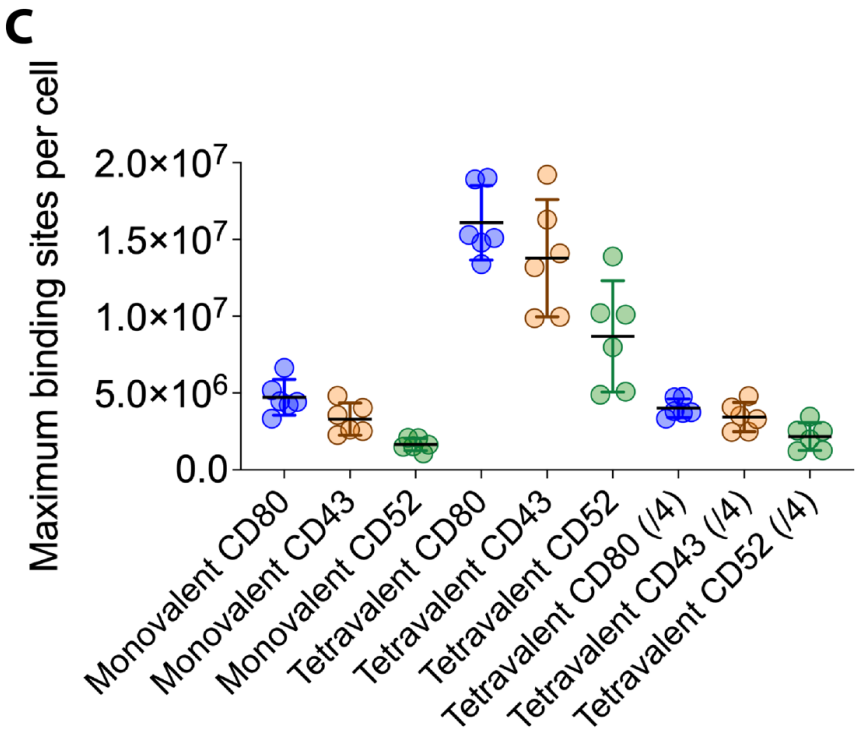
C
Maximum binding sites per cell
2.0×10^7
1.5×10^7
1.0×10^7
5.0×10^6
0.0
Monovalent CD80
Monovalent CD43
Monovalent CD52
Tetravalent CD80
Tetravalent CD43
Tetravalent CD52
Tetravalent CD80 (/4)
Tetravalent CD43 (/4)
Tetravalent CD52 (/4)

sFigure 5

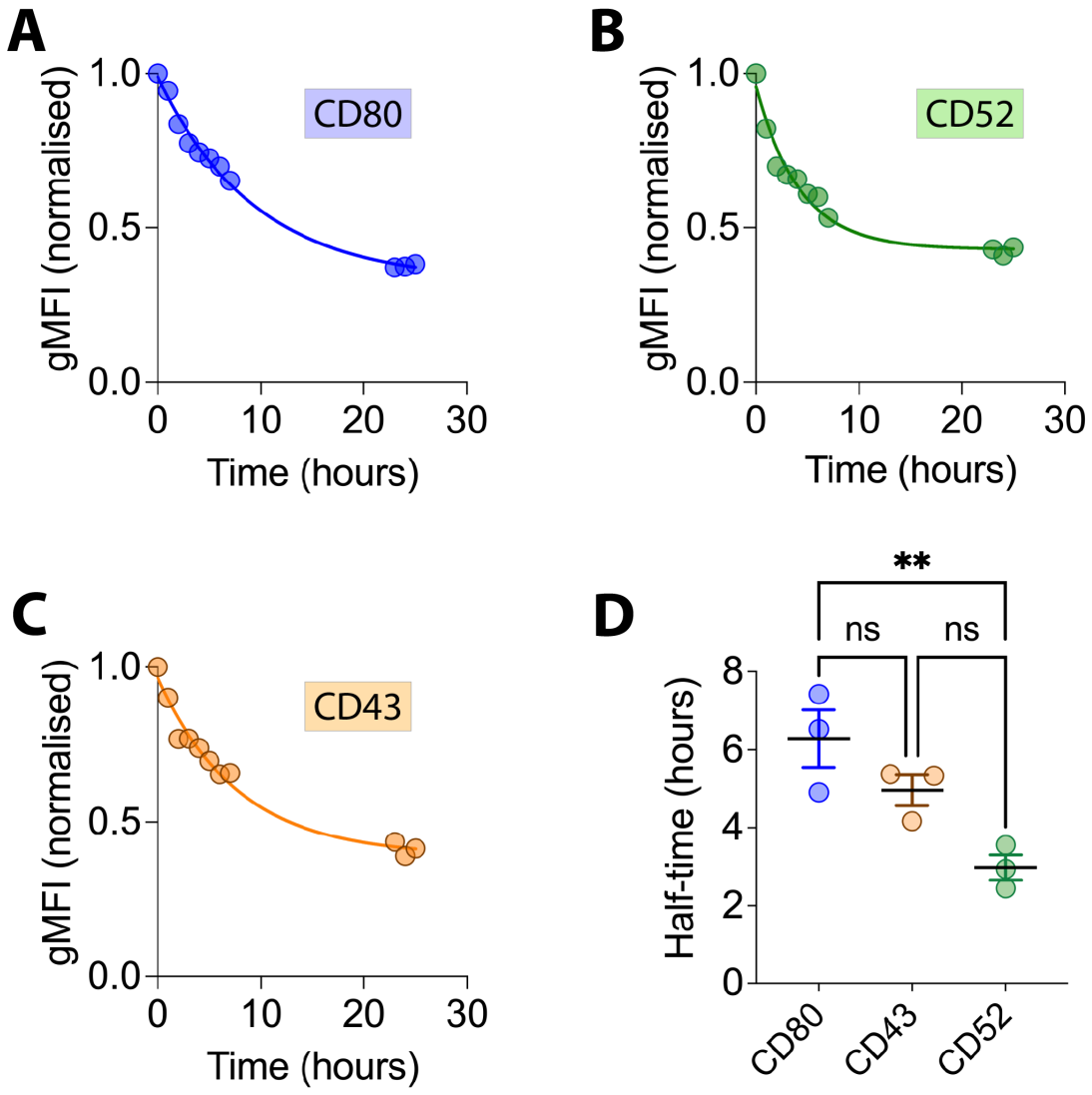
A
CD80
gMFI (normalised)
1.0
0.5
0.0
0
10
20
30
Time (hours)
B
CD52
gMFI (normalised)
1.0
0.5
0.0
0
10
20
30
Time (hours)
C
CD43
gMFI (normalised)
1.0
0.5
0.0
0
10
20
30
Time (hours)
D
**
ns
ns
Half-time (hours)
8
6
4
2
0
CD80
CD43
CD52

sFigure 6

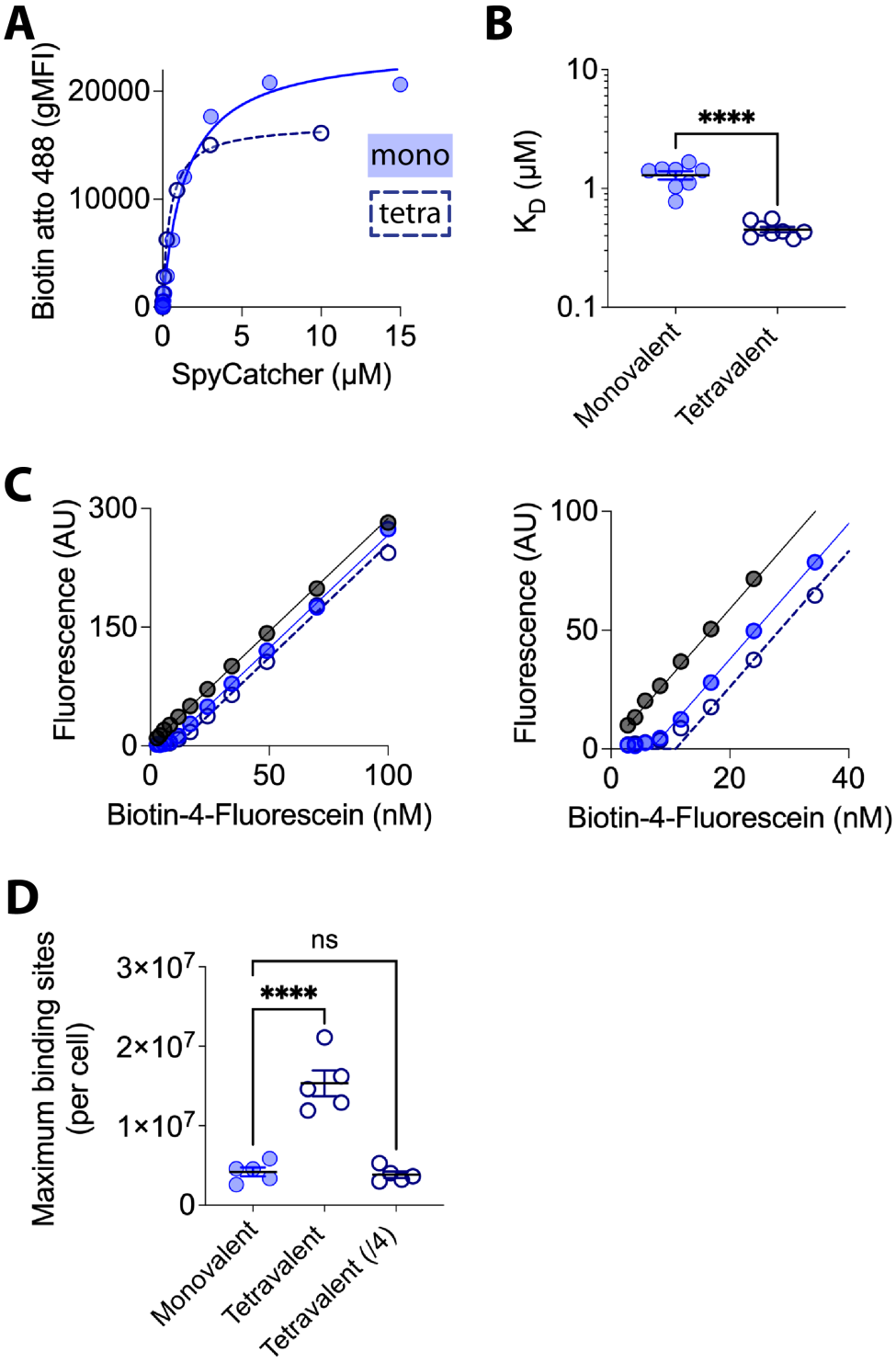
A
Biotin atto 488 (gMFI)
20000
10000
0
0
5
10
15
SpyCatcher (μM)
mono
tetra
B
K_D (μM)
10
1
0.1
****
Monovalent
Tetravalent
C
Fluorescence (AU)
300
150
0
0
50
100
Biotin-4-Fluorescein (nM)
Fluorescence (AU)
100
50
0
0
20
40
Biotin-4-Fluorescein (nM)
D
Maximum binding sites (per cell)
3×10^7
2×10^7
1×10^7
0
ns
****
Monovalent
Tetravalent
Tetravalent (/4)

sFigure 7

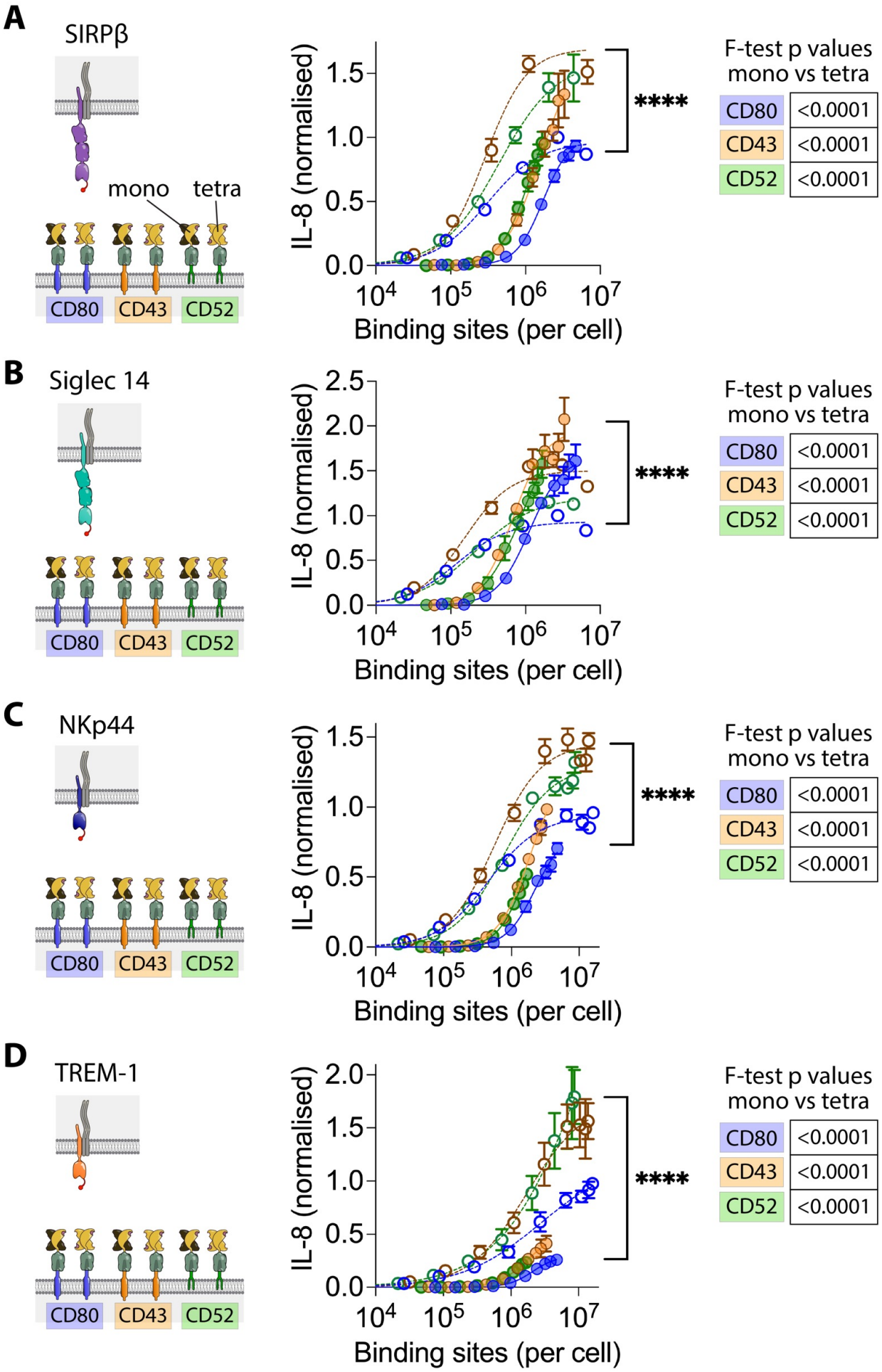
A
SIRPβ
mono
tetra
CD80
CD43
CD52
IL-8 (normalised)
Binding sites (per cell)
****
F-test p values
mono vs tetra
CD80 <0.0001
CD43 <0.0001
CD52 <0.0001
B
Siglec 14
C
NKp44
D
TREM-1

sFigure 8

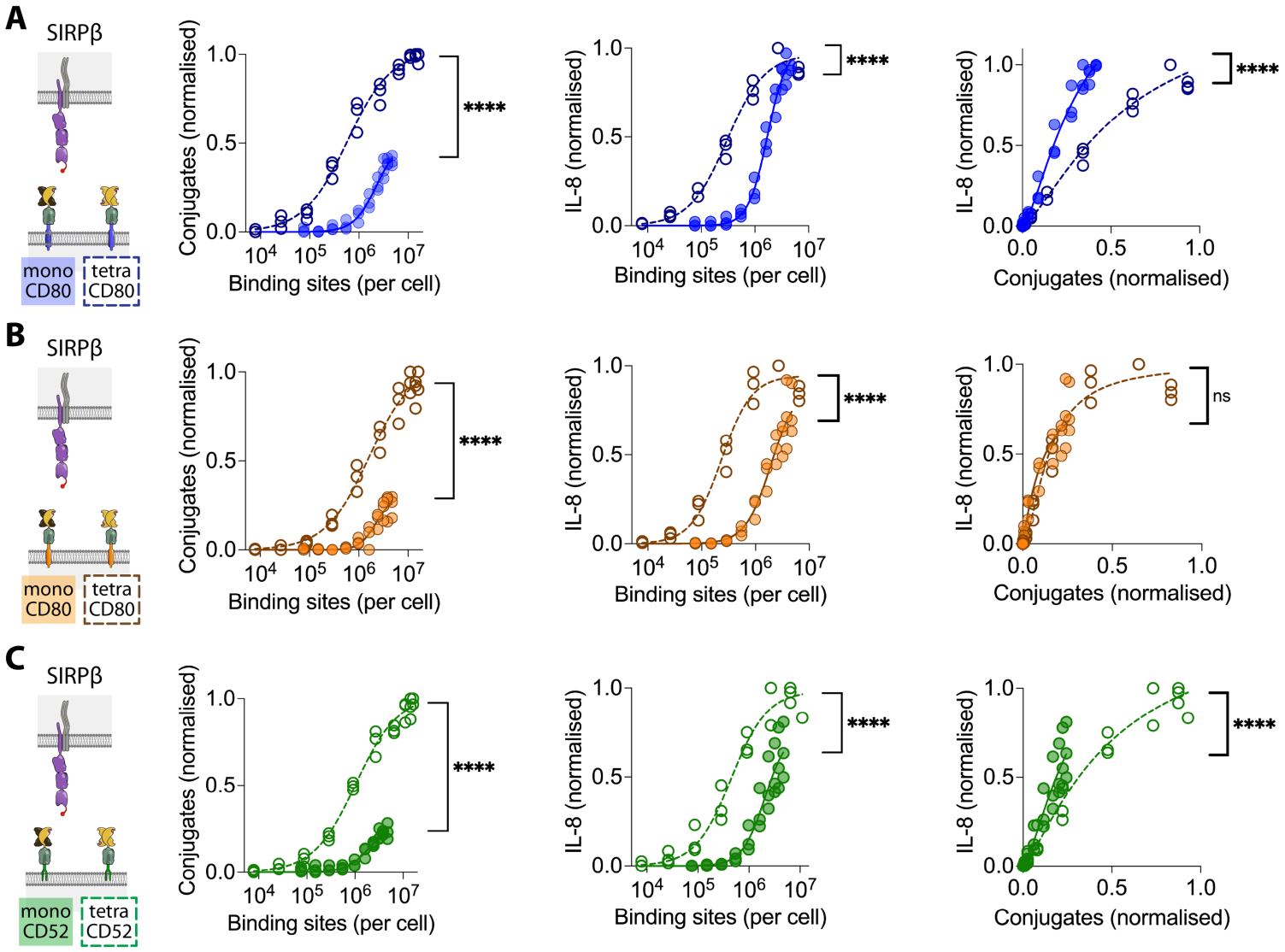
A
SIRPβ
mono CD80
tetra CD80
Conjugates (normalised)
Binding sites (per cell)
IL-8 (normalised)
Conjugates (normalised)
****
B
SIRPβ
mono CD80
tetra CD80
ns
C
SIRPβ
mono CD52
tetra CD52

sFigure 9

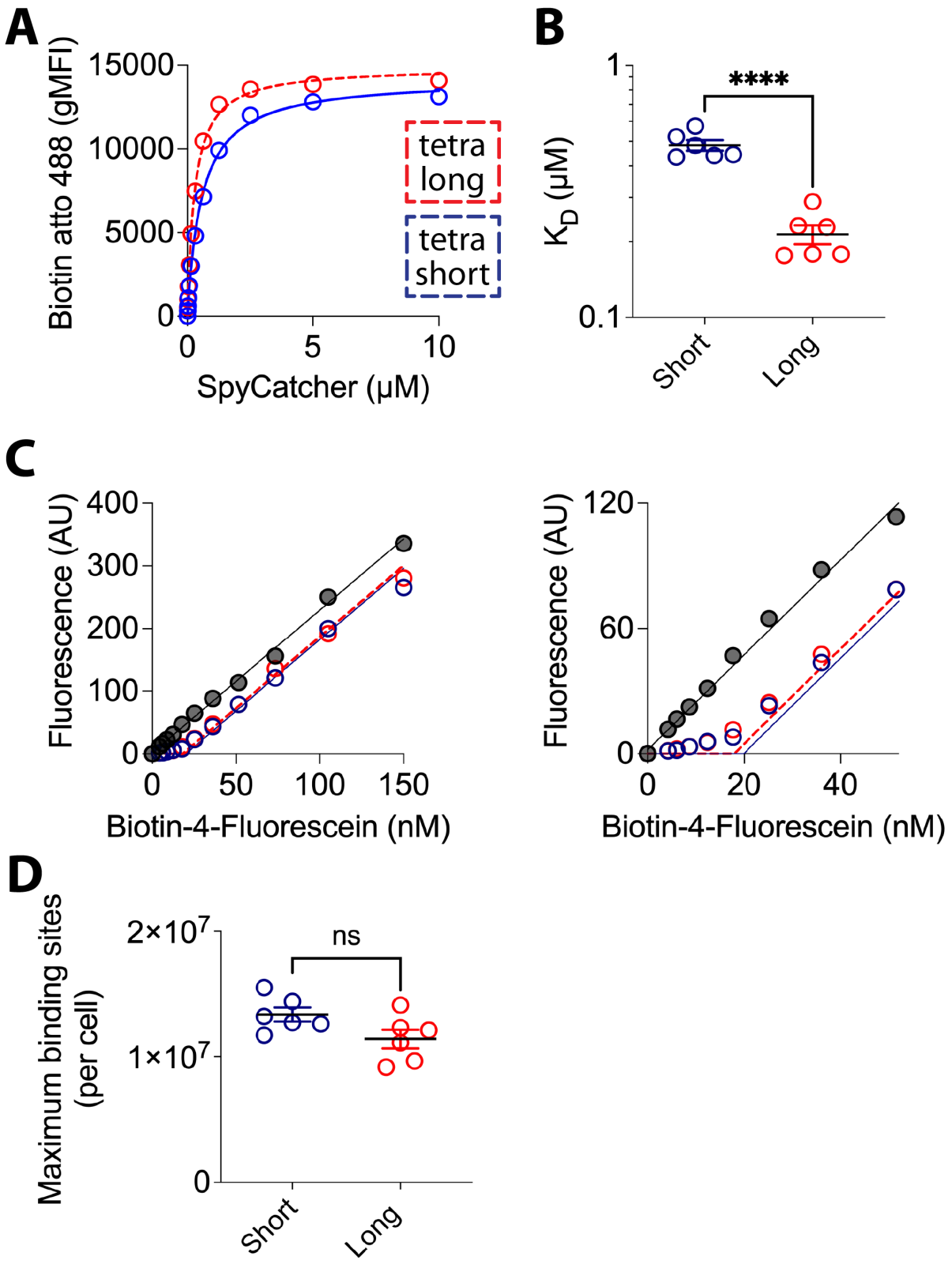
A
Biotin atto 488 (gMFI)
15000
10000
5000
0
0
5
10
SpyCatcher (μM)
tetra long
tetra short
B
K_D (μM)
1
0.1
****
Short
Long
C
Fluorescence (AU)
400
300
200
100
0
0
50
100
150
Biotin-4-Fluorescein (nM)
Fluorescence (AU)
120
60
0
0
20
40
Biotin-4-Fluorescein (nM)
D
Maximum binding sites (per cell)
2×10^7
1×10^7
0
ns
Short
Long